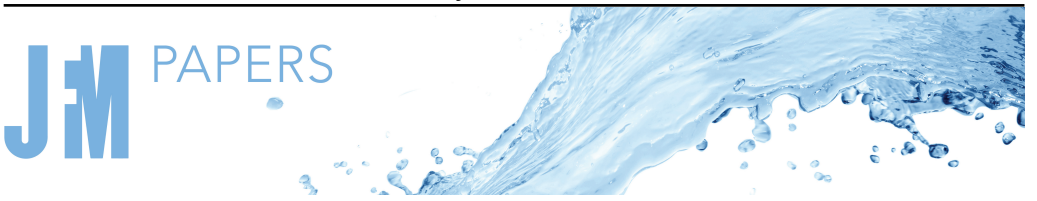
J. Fluid Mech. (2026), *vol.* 1034, A5, doi:10.1017/jfm.2026.11474



Hydrodynamic liquid crystal models for lipid bilayers

Ingo Nitschke[1], **Jan Magnus Sischka**[1] **and Axel Voigt**[1,2,3]

[1]Institut für Wissenschaftliches Rechnen, Technische Universität Dresden, 01062 Dresden, Germany

[2]Center for Systems Biology Dresden (CSBD), Pfotenhauerstr. 108, 01307 Dresden, Germany

[3]Cluster of Excellence Physics of Life (PoL), Technische Universität Dresden, 01062 Dresden, Germany

Corresponding author: Axel Voigt, axel.voigt@tu-dresden.de

(Received 14 December 2025; revised 2 March 2026; accepted 23 March 2026)

Coarse-grained continuous descriptions for lipid bilayers are typically based on minimising the Helfrich energy. Such models consider the fluid properties of these structures only implicitly and have been shown to nicely reproduce equilibrium properties. Model extensions that also address the dynamics of these structures are surface (Navier–)Stokes–Helfrich models. They explicitly account for membrane viscosity. However, these models also usually treat the lipid bilayer as a homogeneous continuum, neglecting the molecular degrees of freedom of the lipids. Here, we derive refined models that consider in addition a scalar order parameter representing the molecular alignment of the lipids along the surface normal. Starting from hydrodynamic surface liquid crystal models, we obtain a hydrodynamic surface Landau–Helfrich model for asymmetric lipid bilayers and a surface Beris–Edwards model for symmetric lipid bilayers. The fully ordered case for both models leads to the known surface (Navier–)Stokes–Helfrich models. Besides more detailed continuous models for lipid bilayers, we therefore also provide an alternative derivation of surface (Navier–)Stokes–Helfrich models. The impact on the dynamics is demonstrated by numerical simulations.

Key words: membranes, liquid crystals

1. Introduction

Lipid bilayers constitute the fundamental structural components of biological membranes. They separate the cell from its exterior and organelles from the cytoplasm. In order to support life, they must balance the competing demands of fluidity versus mechanical

© The Author(s), 2026. Published by Cambridge University Press. This is an Open Access article, distributed under the terms of the Creative Commons Attribution licence (https://creativecommons.org/licenses/by/4.0/), which permits unrestricted re-use, distribution and reproduction, provided the original article is properly cited.

https://doi.org/10.1017/jfm.2026.11474 Published online by Cambridge University Press

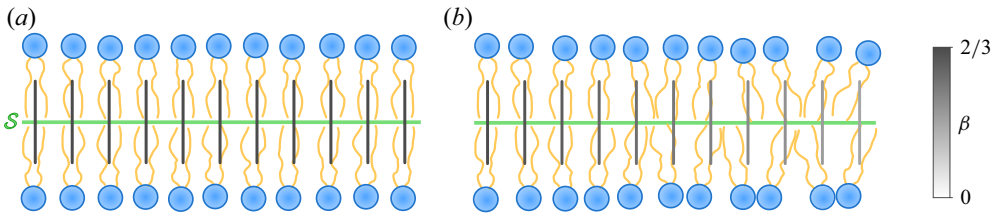


Figure 1. Symmetric lipid bilayer. (*a*) Lipid molecules are in a fully ordered state ($\beta = (2/3)$), i.e. they are perfectly aligned perpendicular to the surface $\mathcal{S}$. (*b*) The degree of orientational order β decreases from left to right, while the mean molecular alignment remains normal to the surface. The bilayer is represented by a surface $\mathcal{S}$ (green line) and the molecular orientation by a Q-tensor field $\boldsymbol{Q}$ fulfilling ansatz (4.1), i.e. $\boldsymbol{Q}$ is depicting an apolar normal field (grey rods) with order parameter β (greyscale). For $\beta \neq 0$, the lipid molecules are not in an isotropic state, the geometric minimal configuration is obtained by minimising the Helfrich energy with zero spontaneous curvature, thus leading to a flat surface.

robustness and permeability. Eukaryotic organisms solve this problem through lipid ordering. While considered in microscopic modelling approaches, continuous descriptions of lipid bilayers typically lack such information. The classical Helfrich model (Helfrich 1973) provides the cornerstone for understanding the continuum mechanics of fluidic membranes by introducing a curvature-elastic bending energy characterised by mean and Gaussian curvature moduli and a spontaneous curvature, as well as constraints, e.g. on enclosed volume and/or global area or local inextensibility. While this model successfully captures equilibrium properties of lipid bilayers (Seifert 1997), typically used gradient flows of the energy to evolve towards the equilibrium cannot, at least not quantitatively, describe the time-dependent, hydrodynamic evolution of biological membranes. Over the past decades, various extensions have been proposed to couple the Helfrich energy with surface fluid dynamics, typically within the framework of inextensible viscous surfaces. Such models for fluid deformable surfaces account for membrane viscosity (Dimova *et al.* 2006; Faizi, Dimova & Vlahovska 2021) and consider surface Navier–Stokes equations (Reuther, Nitschke & Voigt 2020; Krause & Voigt 2023; Olshanskii 2023; Sischka, Nitschke & Voigt 2025; Sauer 2025) or their Stokes limit (Arroyo & DeSimone 2009; Torres-Sánchez *et al.* 2019; Zhu, Saintillan & Chern 2025) coupled with bending properties. With this solid–fluid duality any shape change contributes to tangential flow and *vice versa* any tangential flow on a curved surface induces shape deformations. However, these models usually treat the biological membrane as a homogeneous continuum, neglecting the molecular degrees of freedom that can influence local curvature and flow resistance and, therefore, the balance between fluidity and robustness. A complementary perspective arises from liquid crystal hydrodynamics, particularly the Beris–Edwards framework (Beris & Edwards 1994), which describes the dynamics of nematic order through the evolution of a Q-tensor field coupled to hydrodynamic motion. Surface formulations of these models have recently been developed to study active and passive nematic layers on curved surfaces (Nitschke & Voigt 2025*a*,*b*). While these approaches provide a rigorous treatment of orientational order and its relaxation, they primarily apply to systems with an inherent up–down symmetry, e.g., nematic shells, or, if the average molecule directions are constrained to be perpendicular to the surface, symmetric lipid bilayers, cf. figure 1, and thus, cannot capture asymmetry characteristics of biological membranes, where the asymmetry emerges from different molecular compositions, different molecular densities or due to scaffolding protein, cf. figure 2. For more detailed discussions and the origin of asymmetry in biological membranes, see McMahon & Gallop (2005).

In this work we introduce a hydrodynamic Landau–Helfrich (LH) model that bridges these two perspectives. Building on a polarised Landau–de Gennes energy defined on

https://doi.org/10.1017/jfm.2026.11474 Published online by Cambridge University Press

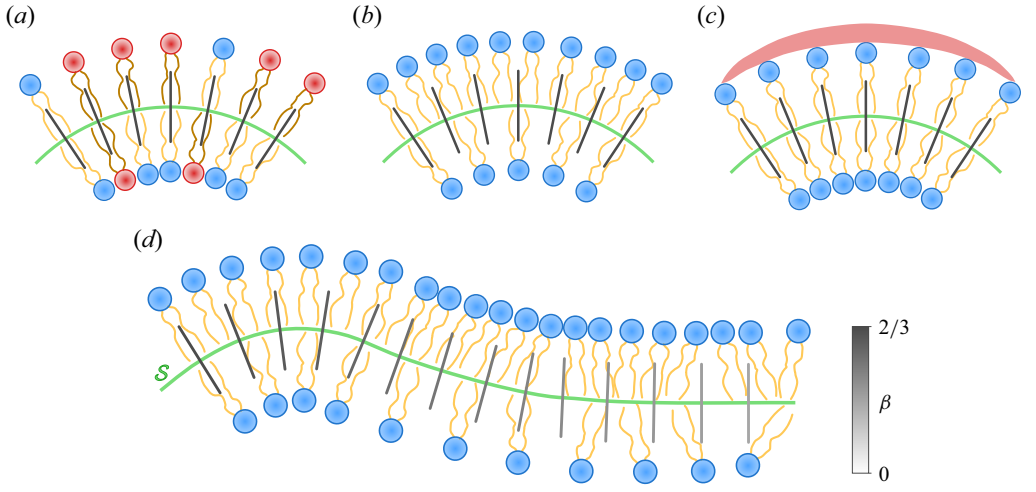


Figure 2. Asymmetric lipid bilayer. The asymmetry may arise through various mechanisms. We provide some examples. (*a*) Differing molecular compositions. (*b*,*d*) Differing molecular densities. (*c*) Scaffold protein. The molecular orientation is represented by a Q-tensor field $\boldsymbol{Q}$ fulfilling ansatz (4.1), i.e. $\boldsymbol{Q}$ is depicting an apolar normal field (grey rods) with order parameter β (greyscale). (*a*,*b*,*c*) In the ordered state ($\beta = (2/3)$), with all lipid molecules aligned normal to the surface $\mathcal{S}$ (green curve), the minimal geometric configuration is achieved when the mean curvature takes its spontaneous curvature value ($\mathcal{H}_0$). (*d*) A less ordered non-uniform state ($\beta < (2/3)$) may counteract this effect, since another spontaneous curvature ($\hat{\mathcal{H}}_0$) related to the isotropic state ($\beta = 0$) can be imposed additionally. The geometric minimal configuration is achieved for a curved surface with the mean curvature depending on β, $\mathcal{H}_0$ and $\hat{\mathcal{H}}_0$.

moving surfaces, we derive a self-consistent model that couples the hydrodynamics of an inextensible viscous surface to a scalar order parameter representing the molecular alignment along the surface normal. The model is obtained through the Lagrange–d'Alembert principle for moving surfaces (Nitschke & Voigt 2025*b*), ensuring consistency between energy variations, viscous dissipation and inextensibility constraints. The polarisation of the Landau–de Gennes energy introduces curvature-order coupling terms that break up–down symmetry and thereby recover the characteristic features of asymmetric lipid bilayers, such as curvature-dependent spontaneous bending. The resulting system consists of generalised surface Navier–Stokes equations coupled to a Landau-type relaxation equation for the order parameter. It admits several important limiting cases: for vanishing polarisation, the equations lead to a special case of the surface Beris–Edwards models (Nitschke & Voigt 2025*b*), which allows one to model symmetric lipid bilayers, and for constant order, the equations reduce to the surface (Navier-)Stokes-Helfrich model for fluid deformable surfaces (Arroyo & DeSimone 2009; Torres-Sánchez *et al.* 2019; Reuther *et al.* 2020). In any of these derived models the bending properties of the models are not specified but result from the underlying liquid crystal interactions and in the special case of the surface (Navier–)Stokes–Helfrich model thus differ from previous derivations. The model formulations are expressed entirely in an observer- and coordinate-invariant tensor calculus suitable for numerical discretisation and analysis within standard (Arbitrary Lagrangian–Eulerian) surface finite-element frameworks (Nestler, Nitschke & Voigt 2019; Sauer 2025). We note that the dependence on the scalar order parameter prevents us from neglecting the effect of Gaussian curvature, despite its purely intrinsic nature. By connecting geometric surface hydrodynamics with molecular ordering through a thermodynamically consistent variational framework, the LH model

https://doi.org/10.1017/jfm.2026.11474 Published online by Cambridge University Press

provides a unified continuum description of asymmetric lipid bilayers that naturally incorporates curvature-order interactions, spontaneous asymmetry and dissipative relaxation. This work thus extends the classical Helfrich theory into a fully hydrodynamic regime, paving the way for systematic investigations of dynamic bilayer processes such as vesicle remodelling, protein-induced curvature generation and the coupling of molecular ordering to membrane flow. While we mainly focus on the liquid-ordered state, phase coexistence between liquid-ordered and liquid-disordered states, as in Baumgart, Hess & Webb (2003), can also be addressed with the proposed hydrodynamic LH model.

The paper is structured as follows: In § 2 we give an overview of mathematical notations relevant for this work. Various models are listed in § 3, comprising the surface Beris–Edwards model for symmetric lipid bilayers (§ 3.1), the hydrodynamic surface LH model for asymmetric lipid bilayers (§ 3.2) and the surface Navier–Stokes–Helfrich model (§ 3.3) as a special case of the previous models for fully ordered lipid bilayers. The derivation of these models is largely carried out in § 4. We propose a Q-tensor ansatz (§ 4.1) for lipid molecules whose average orientation is normal to the surface. The substitution of this ansatz into the surface-conforming Beris–Edwards model (§ 4.2) yields a model for symmetric lipid bilayers. In contrast, we also formulate a polarised surface Landau–de Gennes energy for asymmetric bilayers (§ 4.3), which, upon variation, leads to the hydrodynamic surface LH model. In § 5 numerical results demonstrate the differences in the dynamics if compared with surface Navier–Stokes-Helfrich models. Furthermore, a summary is provided, conclusions are drawn and possible model extensions are discussed. Appendix E provides additional information.

2. Notation and preliminaries

We briefly summarise the most important notation relevant for this paper. We assume that the time-dependent moving surface $\mathcal{S} \subset \mathbb{R}^3$ is sufficiently smooth and parameterisable into the three-dimensional Euclidean space. Tensor fields in $T^n\mathbb{R}^3|_\mathcal{S}$ are considered exclusively on the surface. Coordinate invariance, and the resulting freedom in the choice of frame, allow for an interpretation as a Cartesian frame for the tensor fields. For instance, we could write $\boldsymbol{W} = W^A \boldsymbol{e}_A$ (Einstein summation) with $A \in \{x, y, z\}$ for a vector, respectively one-tensor field $\boldsymbol{W} \in T\mathbb{R}^3|_\mathcal{S} := T^1\mathbb{R}^3|_\mathcal{S}$. A special vector field is the normal field $\boldsymbol{\nu} \in T\mathbb{R}^3|_\mathcal{S}$ perpendicular to the surface and normalised. It spans a one-dimensional subvector field space, whose orthogonal complement consists of the tangential vector fields $T\mathcal{S} < T\mathbb{R}^3|_\mathcal{S}$. The associated projection is given by the surface identity tensor field $\boldsymbol{Id}_\mathcal{S}$, i.e. it is $T\mathcal{S} = \boldsymbol{Id}_\mathcal{S} T\mathbb{R}^3|_\mathcal{S}$ valid. This concept readily scales to n-tensor fields $T^n\mathbb{R}^3|_\mathcal{S}$ and tangential n-tensor fields $T^n\mathcal{S} < T^n\mathbb{R}^3|_\mathcal{S}$. The surface identity tensor field $\boldsymbol{Id}_\mathcal{S} \in T^2\mathcal{S}$ is such a tangential tensor field and could be represented by $\boldsymbol{Id}_\mathcal{S} = \boldsymbol{Id} - \boldsymbol{\nu} \otimes \boldsymbol{\nu}$, or the metric tensor of an arbitrary local tangential frame, where $\boldsymbol{Id} \in T^2\mathbb{R}^3|_\mathcal{S}$ is the usual Euclidean identity tensor field, e.g. given by $\delta^{AB}\boldsymbol{e}_A \otimes \boldsymbol{e}_B$ with respect to a Cartesian frame. We repeatedly make use of the corresponding orthogonal decompositions. Force fields $\boldsymbol{F} = \boldsymbol{f} + f^\perp_{\boldsymbol{\nu}} \in T\mathbb{R}^3|_\mathcal{S}$, for instance, are decomposable into a tangential force field $\boldsymbol{f} = \boldsymbol{Id}_\mathcal{S}\boldsymbol{F} \in T\mathcal{S}$ and a scalar-valued normal force field $f^\perp = \boldsymbol{\nu}\boldsymbol{F} \in T^0\mathcal{S}$, or, stress fields

$$\boldsymbol{\Sigma} = \boldsymbol{\sigma} + \boldsymbol{\nu} \otimes \boldsymbol{\eta} \in T\mathbb{R}^3|_\mathcal{S} \otimes T\mathcal{S} < T^2\mathbb{R}^3|_\mathcal{S} \tag{2.1}$$

are usually right tangential and decomposed into a tangential stress field $\boldsymbol{\sigma} = \boldsymbol{Id}_\mathcal{S}\boldsymbol{\Sigma} \in T^2\mathcal{S}$ and a vector-valued normal(-tangential) stress field $\boldsymbol{\eta} = \boldsymbol{\nu}\boldsymbol{\Sigma} \in T\mathcal{S}$. Furthermore, our framework also involves Q-tensor fields in $\mathcal{Q}^2\mathbb{R}^3|_\mathcal{S} := \{\boldsymbol{Q} \in T^2\mathbb{R}^3|_\mathcal{S} \mid \boldsymbol{Q} = \boldsymbol{Q}^T \text{ and } \operatorname{Tr}\boldsymbol{Q} = 0\}$ and tangential Q-tensor fields in $\mathcal{Q}^2\mathcal{S} := \{\boldsymbol{q} \in T^2\mathcal{S} \mid \boldsymbol{q} = \boldsymbol{q}^T \text{ and}$

https://doi.org/10.1017/jfm.2026.11474 Published online by Cambridge University Press

$\mathrm{Tr}\boldsymbol{q} = 0\} \leq \mathcal{Q}^2\mathbb{R}^3|_{\mathcal{S}}$, also known as flat-degenerated Q-tensor fields. A complete orthogonal decomposition of $\mathcal{Q}^2\mathbb{R}^3|_{\mathcal{S}}$ is given in (4.2).

The local inner product is denoted by angle brackets, i.e. $\langle\cdot,\cdot\rangle_{\mathcal{V}} : \mathcal{V}\times\mathcal{V}\to T^0\mathcal{S}$, where $\mathcal{V}\leq T^n\mathbb{R}^3|_{\mathcal{S}}$. A specification of the frame is not needed as coordinate invariance and the properties of subvector spaces guarantee that the results remain consistent. For instance, $\langle\boldsymbol{v},\boldsymbol{w}\rangle_{T\mathcal{S}} = \langle\boldsymbol{v},\boldsymbol{w}\rangle_{T\mathbb{R}^3|_{\mathcal{S}}} = \boldsymbol{v}\boldsymbol{w} = g_{ij}v^i w^j = v^i w_i = \delta_{AB}v^A w^B$ is valid for all $\boldsymbol{v},\boldsymbol{w}\in T\mathcal{S}$. The global inner product is defined in terms of the corresponding local one: $\langle\cdot,\cdot\rangle := \int_{\mathcal{S}}\langle\cdot,\cdot\rangle_{\mathcal{V}}\,\mathrm{d}\mathcal{S} : \mathcal{V}\times\mathcal{V}\to\mathbb{R}$. All norms are defined as those induced by the inner products: $\|\cdot\|_\bullet^2 := \langle\cdot,\cdot\rangle_\bullet$.

We use the componentwise derivative $\boldsymbol{\nabla}_{\mathsf{C}} : T^n\mathbb{R}^3|_{\mathcal{S}}\to T^n\mathbb{R}^3|_{\mathcal{S}}\otimes T\mathcal{S} < T^{n+1}\mathbb{R}^3|_{\mathcal{S}}$ as the starting point for derivatives on tensor fields, since it captures all possible first-order derivative information with respect to the ambient Euclidean space. In principle, it is the ordinary $\mathbb{R}^3$-derivative modulo the normal derivative, i.e. $\boldsymbol{\nabla}_{\mathsf{C}} = (\boldsymbol{Id}_{\mathcal{S}}\boldsymbol{\nabla}_{\mathbb{R}^3})|_{\mathcal{S}}$, should one wish to consider extensions in the normal direction, although $\boldsymbol{\nabla}_{\mathsf{C}}$ is invariant with respect to any sufficiently smooth normal extension. If we use an arbitrary tangential frame $\{\partial_i\boldsymbol{X}\mid i=1,2\}$, we could define $\boldsymbol{\nabla}_{\mathsf{C}}\boldsymbol{R} := g^{ik}(\partial_k\boldsymbol{R})\otimes\partial_i\boldsymbol{X}$ for all $\boldsymbol{R}\in T^n\mathbb{R}^3|_{\mathcal{S}}$, where g^{ik} yields the contravariant proxy of the metric tensor, also known as the inverse metric tensor, with respect to the chosen frame. Equivalently, it holds that $[\boldsymbol{\nabla}_{\mathsf{C}}\boldsymbol{R}]^{A_1\ldots A_nB}\boldsymbol{e}_B = \boldsymbol{\nabla}R^{A_1\ldots A_n}$ for $\boldsymbol{R} = R^{A_1\ldots A_n}\boldsymbol{e}_{A_1}\otimes\ldots\otimes\boldsymbol{e}_{A_n}$ in a Cartesian frame and covariant derivative $\boldsymbol{\nabla}$ on scalar fields. The shape operator $\boldsymbol{II}\in T^2\mathcal{S}$, also known as the second fundamental form, follows directly from this via $\boldsymbol{II} = -\boldsymbol{\nabla}_{\mathsf{C}}\boldsymbol{\nu}$. Other curvature related quantities derived from this are the mean curvature $\mathcal{H} = \mathrm{Tr}\boldsymbol{II} = \boldsymbol{Id}_{\mathcal{S}} : \boldsymbol{II}$ and the Gaussian curvature $\mathcal{K} = (1/2)(\mathcal{H}^2 - \|\boldsymbol{II}\|^2_{T^2\mathcal{S}})$, the two scalar-valued invariants of the shape operator. With respect to a local tangential frame, it also holds that $\mathcal{K} = \det\{II^i_j\}$ or $\mathcal{K} = (1/4)\boldsymbol{E} : \boldsymbol{\mathcal{R}} : \boldsymbol{E}$, where $\boldsymbol{E}\in T^2\mathcal{S}$ is the Levi-Civita and $\boldsymbol{\mathcal{R}}\in T^4\mathcal{S}$ is the Riemann curvature tensor field. On scalar fields the componentwise and covariant derivative are the same, i.e. $\boldsymbol{\nabla}_{\mathsf{C}} = \boldsymbol{\nabla} : T^0\mathcal{S}\to T\mathcal{S}$. This is not generally valid, not even for tangential tensor fields. For a vector field $\boldsymbol{V} = \boldsymbol{v} + v_\perp\boldsymbol{\nu}\in T\mathbb{R}^3|_{\mathcal{S}}$, e.g. $\boldsymbol{\nabla}_{\mathsf{C}}\boldsymbol{V} = \boldsymbol{\nabla}\boldsymbol{v} - v_\perp\boldsymbol{II} + \boldsymbol{\nu}\otimes(\boldsymbol{\nabla}v_\perp + \boldsymbol{II}\,\boldsymbol{v})$ holds. As the divergence operator, we use the componentwise trace divergence $\mathrm{Div}_{\mathsf{C}} := \mathrm{Tr}\circ\boldsymbol{\nabla}_{\mathsf{C}}$, where the trace applies on the two rear column dimensions, including the derivative acting on the last index. It should be noted that the trace divergence equals the L^2 adjoint $-\boldsymbol{\nabla}^*_{\mathsf{C}}$ only for right-tangential tensor fields, since the correct relation is $\mathrm{Div}_{\mathsf{C}}\boldsymbol{R} = -(\boldsymbol{\nabla}^*_{\mathsf{C}}\boldsymbol{R} + \mathcal{H}\boldsymbol{R}\boldsymbol{\nu})$ for all $\boldsymbol{R}\in T^n\mathbb{R}^3|_{\mathcal{S}}$. Fortunately, this is true for fluid stress fields (2.1) in this paper, e.g. it holds that $\langle\mathrm{Div}_{\mathsf{C}}\boldsymbol{\Sigma},\boldsymbol{W}\rangle_{\mathrm{L}^2(T\mathbb{R}^3|_{\mathcal{S}})} = -\langle\boldsymbol{\Sigma},\boldsymbol{\nabla}_{\mathsf{C}}\boldsymbol{W}\rangle_{\mathrm{L}^2(T^2\mathbb{R}^3|_{\mathcal{S}})}$ in that case for all $\boldsymbol{W}\in T\mathbb{R}^3|_{\mathcal{S}}$. However, at least for pressure gradients, we need the L^2 adjoint of the trace divergence. This gives rise to the adjoint gradient $\mathrm{Grad}_{\mathsf{C}} := -\mathrm{Div}^*_{\mathsf{C}}$, which yields the relation $\mathrm{Grad}_{\mathsf{C}}\boldsymbol{R} = \boldsymbol{\nabla}_{\mathsf{C}}\boldsymbol{R} + \mathcal{H}\boldsymbol{R}\otimes\boldsymbol{\nu}$ for all $\boldsymbol{R}\in T^n\mathbb{R}^3|_{\mathcal{S}}$ as a consequence. The key representations in the covariant differential calculus relevant to this paper are $\mathrm{Div}_{\mathsf{C}}\boldsymbol{\Sigma} = \mathrm{div}\boldsymbol{\sigma} - \boldsymbol{II}\,\boldsymbol{\eta} + (\mathrm{div}\boldsymbol{\eta} + \boldsymbol{II} : \boldsymbol{\sigma})\boldsymbol{\nu}$ for right-tangential fields (2.1), $\mathrm{Div}_{\mathsf{C}}\boldsymbol{V} = \mathrm{div}\boldsymbol{v} - \mathcal{H}v_\perp$ for vector fields $\boldsymbol{V} = \boldsymbol{v} + v_\perp\boldsymbol{\nu}\in T\mathbb{R}^3|_{\mathcal{S}}$ and $\mathrm{Grad}_{\mathsf{C}}p = \mathrm{Div}_{\mathsf{C}}(p\boldsymbol{Id}_{\mathcal{S}}) = \boldsymbol{\nabla}p + p\mathcal{H}\boldsymbol{\nu}$ for scalar fields $p\in T^0\mathcal{S}$.

Even if our focus is not on the numerical solution of the proposed models, we consider $\mathbb{R}^3$ representations with componentwise differential operators as they are the most convenient for standard numerical implementations, e.g. by the surface finite element method. First, the operators act directly on the Cartesian proxy of the material velocity (e.g. $\mathrm{Div}_{\mathsf{C}}\boldsymbol{V} = (\delta^B_A - \nu_A\nu^B)\partial_B V^A$ for $A,B\in\{x,y,z\}$). Second, differential operators

https://doi.org/10.1017/jfm.2026.11474 Published online by Cambridge University Press

straightforwardly admit a weak formulation due to the L^2-adjoint relations

$$\begin{aligned}\langle \mathrm{Div}_{\mathsf{C}} \boldsymbol{\Sigma}, \boldsymbol{W}\rangle_{\mathrm{L}^2(T\mathbb{R}^3|_{\mathcal{S}})} &= -\langle \boldsymbol{\Sigma}, \nabla_{\mathsf{C}} \boldsymbol{W}\rangle_{\mathrm{L}^2(T^2\mathbb{R}^3|_{\mathcal{S}})}\,,\\ \langle \mathrm{Div}_{\mathsf{C}} \boldsymbol{W}, \psi\rangle_{\mathrm{L}^2(T^0\mathcal{S})} &= -\langle \boldsymbol{W}, \mathrm{Grad}_{\mathsf{C}} \psi\rangle_{\mathrm{L}^2(T\mathbb{R}^3|_{\mathcal{S}})}\,,\end{aligned} \tag{2.2}$$

for all $\boldsymbol{\Sigma} \in T\mathbb{R}^3|_{\mathcal{S}} \otimes T\mathcal{S}$, $\boldsymbol{W} \in T\mathbb{R}^3|_{\mathcal{S}}$ and $\psi \in T^0\mathcal{S}$. For a more comprehensive overview on tensor calculus on moving surfaces, see the introduction chapter in Nitschke (2025) or the detailed mathematical introductions with respect to time derivatives in Nitschke & Voigt (2023), with respect to energy variations in Nitschke, Sadik & Voigt (2023) and with respect to the Lagrange–d'Alembert principle in Nitschke & Voigt (2025*b*).

3. Models

3.1. *Surface Beris–Edwards model for symmetric lipid bilayers*

A hydrodynamic liquid crystal model for symmetric lipid bilayers can be obtained from the surface Beris–Edwards framework (Nitschke & Voigt 2025*b*). We carry out this derivation in § 4.2 starting from the surface-conforming Beris–Edwards model (Nitschke & Voigt 2025*b*) (§ 3.3), conveniently provided in Appendix D. This leads to the following assertion.

Find the material velocity field $\boldsymbol{V} \in T\mathbb{R}^3|_{\mathcal{S}}$, scalar field $\beta \in T^0\mathcal{S}$ and generalised pressure field $\tilde{p} \in T^0\mathcal{S}$ such that

$$\rho\,(\partial_t \boldsymbol{V} + (\nabla_{\mathsf{C}} \boldsymbol{V})\,(\boldsymbol{V} - \boldsymbol{V}_{\mathfrak{o}})) = \mathrm{Grad}_{\mathsf{C}}\,\tilde{p} + \mathrm{Div}_{\mathsf{C}}\,\tilde{\boldsymbol{\Sigma}}$$

$$\begin{aligned}\text{with}\quad \tilde{\boldsymbol{\Sigma}} = {}& \upsilon\left(1+\frac{\xi}{2}\beta\right)^2\left(\boldsymbol{Id}_{\mathcal{S}}\nabla_{\mathsf{C}}\boldsymbol{V} + (\boldsymbol{Id}_{\mathcal{S}}\nabla_{\mathsf{C}}\boldsymbol{V})^T\right) - \frac{3L}{2}\left(\nabla_{\mathsf{C}}\beta\otimes\nabla_{\mathsf{C}}\beta + 3\beta^2\mathcal{H}\boldsymbol{II}\right)\\ &+ \frac{9}{2}\boldsymbol{v}\otimes\left(\delta^{\Phi}_{\mathfrak{m}} M\beta^2\boldsymbol{v}\nabla_{\mathsf{C}}\boldsymbol{V} - L\beta\,(\beta\nabla_{\mathsf{C}}\mathcal{H} + 2\boldsymbol{II}\nabla_{\mathsf{C}}\beta)\right), \qquad (3.1a)\end{aligned}$$

$$\begin{aligned}&\left(M + \frac{\upsilon\xi^2}{2}\right)(\partial_t\beta + (\nabla_{\mathsf{C}}\beta)\,(\boldsymbol{V} - \boldsymbol{V}_{\mathfrak{o}}))\\ &= L\left(\Delta_{\mathsf{C}}\beta - 3\beta\left(\mathcal{H}^2 - 2\mathcal{K}\right)\right) - \left(2a + b\beta + 3c\beta^2\right)\beta, \qquad (3.1b)\end{aligned}$$

$$\mathrm{Div}_{\mathsf{C}}\boldsymbol{V} = 0 \qquad (3.1c)$$

holds for $\dot{\rho} = 0$ and given initial conditions for $\boldsymbol{V}$, β and mass density $\rho \in T^0\mathcal{S}$.

Here $\boldsymbol{V}_{\mathfrak{o}} \in T\mathbb{R}^3|_{\mathcal{S}}$ is the so-called observer velocity, which is arbitrary, not necessarily divergence free, and could be used as mesh velocity in a discretised problem for instance. We use $\beta \in T^0\mathcal{S}$ as a proxy for the scalar order parameter $S \in T^0\mathcal{S}$. In fact, β is the eigenvalue of the corresponding Q-tensor field in the normal direction. Ultimately, β statistically quantifies the degree to which the lipid molecules are aligned along the normal direction: $\beta = (2/3)$ for the fully ordered state and $\beta = 0$ for the isotropic, i.e. disordered, state. In this process, the average molecular orientation is constant along the normal direction. The fluid stress tensor $\tilde{\boldsymbol{\Sigma}} \in T\mathbb{R}^3|_{\mathcal{S}} \otimes T\mathcal{S}$ is given modulo $\boldsymbol{Id}_{\mathcal{S}}$; the resulting pressure gradient is, respectively, incorporated into the generalised pressure $\tilde{p}$. Material parameters are the isotropic viscosity υ, anisotropy coefficient ξ, elastic parameter L, immobility coefficient M and thermotropic coefficients a, b and c; cf. table 3. The Kronecker delta $\delta^{\Phi}_{\mathfrak{m}}$ acts as a switch that selects between the material model ($\Phi = \mathfrak{m}$: $\delta^{\Phi}_{\mathfrak{m}} = 1$) and the Jaumann model ($\Phi = \mathcal{J}$: $\delta^{\Phi}_{\mathfrak{m}} = 0$). This distinction is less relevant here than in the more general Beris–Edwards models (Nitschke & Voigt 2025*b*). However, the resulting material immobility force accounts for changes of orientations of the lipids due to the motion of the surface with respect to the surrounding three-dimensional space.

https://doi.org/10.1017/jfm.2026.11474 Published online by Cambridge University Press

This may become relevant if one intends to include the mass, and hence, local torque, of the lipid molecules. The Jaumann model, on the other hand, is invariant under rigid-body rotations; see the discussion in Nitschke & Voigt (2025*b*). In any case, for slow and small lipid surfaces, the choice of model will hardly lead to any qualitative difference in the solution. The lack of a spontaneous curvature term reflects the presence of the up–down symmetry of the surface, something that the general surface Beris–Edwards model in Nitschke & Voigt (2025*b*) already exhibits by construction. As a consequence, the model is appropriate for symmetric lipid bilayers.

In Nitschke & Voigt (2025*a*) additional active mechanisms are considered in the derivation of the general surface Beris–Edwards model. These terms do not contribute in the present setting due to inextensibility and the orthogonal alignment of the lipid molecules with respect to the surface. As a consequence, even with these terms, the solutions exhibit a purely dissipative energy evolution.

The governing equations (3.1) can be transformed into a tangential calculus in the usual manner. The tangential and normal fluid forces on the right-hand side of (3.1*a*) yield

$$
\begin{aligned}
&\boldsymbol{Id}_{\mathcal{S}}\left(\mathrm{Grad}_{\mathsf{C}}\,\tilde{p}+\mathrm{Div}_{\mathsf{C}}\,\boldsymbol{\Sigma}\right)\\
&=\boldsymbol{\nabla}\hat{p}+\upsilon\left(1+\frac{\xi}{2}\beta\right)^{2}\left(\Delta\boldsymbol{v}+\mathcal{K}\boldsymbol{v}-2\left(\boldsymbol{II}-\frac{\mathcal{H}}{2}\boldsymbol{Id}_{\mathcal{S}}\right)\boldsymbol{\nabla}v_{\perp}-v_{\perp}\boldsymbol{\nabla}\mathcal{H}\right)\\
&\quad+\upsilon\xi\left(1+\frac{\xi}{2}\beta\right)\left(\boldsymbol{\nabla}\boldsymbol{v}+\boldsymbol{\nabla}^{T}\boldsymbol{v}-2v_{\perp}\boldsymbol{II}\right)\boldsymbol{\nabla}\beta-\frac{3L}{2}\left(\Delta\beta-3\beta\left(\mathcal{H}^{2}-2\mathcal{K}\right)\right)\boldsymbol{\nabla}\beta\\
&\quad+\frac{9M}{2}\delta_{\mathrm{m}}^{\Phi}\beta^{2}\left(\mathcal{K}\boldsymbol{v}-\boldsymbol{II}\left(\boldsymbol{\nabla}v_{\perp}+\mathcal{H}\boldsymbol{v}\right)\right),\\
&\boldsymbol{v}\left(\mathrm{Grad}_{\mathsf{C}}\,\tilde{p}+\mathrm{Div}_{\mathsf{C}}\,\boldsymbol{\Sigma}\right)\\
&=\mathcal{H}\hat{p}+2\upsilon\left(1+\frac{\xi}{2}\beta\right)^{2}\left(\boldsymbol{II}:\boldsymbol{\nabla}\boldsymbol{v}-v_{\perp}\left(\mathcal{H}^{2}-\mathcal{K}\right)\right)-\frac{3L}{4}\left(14\boldsymbol{\nabla}\beta\boldsymbol{II}\boldsymbol{\nabla}\beta-\mathcal{H}\left\|\boldsymbol{\nabla}\beta\right\|^{2}\right)\\
&\quad-\frac{9L}{4}\beta\left(4\boldsymbol{II}:\boldsymbol{\nabla}^{2}\beta+8\boldsymbol{\nabla}\mathcal{H}\boldsymbol{\nabla}\beta+\beta\left(2\Delta\mathcal{H}+\mathcal{H}\left(\mathcal{H}^{2}-4\mathcal{K}\right)\right)\right)\\
&\quad+\frac{9M}{2}\delta_{\mathrm{m}}^{\Phi}\beta\left(\left(\Delta v_{\perp}+\boldsymbol{II}:\boldsymbol{\nabla}\boldsymbol{v}+\boldsymbol{\nabla}_{\boldsymbol{v}}\mathcal{H}\right)\beta+2\left(\boldsymbol{\nabla}v_{\perp}+\boldsymbol{v}\boldsymbol{II}\right)\boldsymbol{\nabla}\beta\right),
\end{aligned}
\tag{3.2}
$$

where $\boldsymbol{V}=\boldsymbol{v}+v_{\perp}\boldsymbol{\nu}$; see § 4.2. For purely aesthetic reasons, we separated the elastic pressure contribution from the pressure $\tilde{p}$ again, i.e. $\tilde{p}=\hat{p}+(3L/4)(\|\boldsymbol{\nabla}\beta\|^{2}+3\mathcal{H}^{2}\beta^{2})$. The tangential and normal material accelerations forces on the left-hand side of (3.1*a*) are

$$
\begin{aligned}
\rho\boldsymbol{a}&=\rho\boldsymbol{Id}_{\mathcal{S}}\left(\partial_{t}\boldsymbol{V}+\left(\boldsymbol{\nabla}_{\mathsf{C}}\boldsymbol{V}\right)\left(\boldsymbol{V}-\boldsymbol{V}_{\mathrm{o}}\right)\right)\\
&=\rho\left(\left(\partial_{t}v^{i}\right)\partial_{i}\boldsymbol{X}_{\mathrm{o}}+\boldsymbol{\nabla}_{\boldsymbol{v}-\boldsymbol{v}_{\mathrm{o}}}\boldsymbol{v}+\boldsymbol{\nabla}_{\boldsymbol{v}}\boldsymbol{v}_{\mathrm{o}}-v_{\perp}\left(\boldsymbol{\nabla}v_{\perp}+2\boldsymbol{II}\,\boldsymbol{v}\right)\right),\\
\rho a_{\perp}&=\rho\boldsymbol{\nu}\left(\partial_{t}\boldsymbol{V}+\left(\boldsymbol{\nabla}_{\mathsf{C}}\boldsymbol{V}\right)\left(\boldsymbol{V}-\boldsymbol{V}_{\mathrm{o}}\right)\right)\\
&=\rho\left(\partial_{t}v_{\perp}+\boldsymbol{\nabla}_{2\boldsymbol{v}-\boldsymbol{v}_{\mathrm{o}}}v_{\perp}+\boldsymbol{II}\left(\boldsymbol{v},\boldsymbol{v}\right)\right),
\end{aligned}
\tag{3.3}
$$

where $\boldsymbol{V}_{\mathrm{o}}=\boldsymbol{v}_{\mathrm{o}}+v_{\perp}\boldsymbol{\nu}$ and $\{\partial_{i}\boldsymbol{X}_{\mathrm{o}}\}$ is the observer frame; see table 5. The inextensibility constraint (3.4*c*) becomes $\mathrm{div}\boldsymbol{v}=v_{\perp}\mathcal{H}$. The fully ordered case ($\beta=(2/3)$) leads to a surface Navier–Stokes–Helfrich model and is discussed in § 3.3.

3.2. *Hydrodynamic surface LH model for asymmetric lipid bilayers*

The hydrodynamic surface LH model for asymmetric lipid bilayers is derived in Appendix B following the Lagrange-D'Alembert principle, and energetic considerations in § 4.3 and Nitschke & Voigt (2025*b*). The model can be written as follows:

https://doi.org/10.1017/jfm.2026.11474 Published online by Cambridge University Press

Identifier	Expression	
$\mathrm{D}_t^{\mathfrak{m}}\, \boldsymbol{V}$	$\partial_t \boldsymbol{V} + (\nabla_{\mathsf{C}} \boldsymbol{V})(\boldsymbol{V} - \boldsymbol{V}_{\mathfrak{o}})$	Material acceleration (Nitschke & Voigt, 2023)
$\tilde{\boldsymbol{\sigma}}_{NV}$	$\upsilon(1 + \frac{\xi}{2}\beta)^2(\boldsymbol{Id}_{\mathcal{S}} \nabla_{\mathsf{C}} \boldsymbol{V} + (\boldsymbol{Id}_{\mathcal{S}} \nabla_{\mathsf{C}} \boldsymbol{V})^T)$	Deviatoric nematic viscous stress (B15)
$\tilde{\boldsymbol{\sigma}}_1$	$-\frac{3L}{2} \nabla_{\mathsf{C}} \beta \otimes \nabla_{\mathsf{C}} \beta$	Part of the LH stress (B4)
$\tilde{\boldsymbol{\sigma}}_0$	$-\frac{9\kappa}{4}\beta^2(\mathcal{H} - \hat{\mathcal{H}}_0 - \frac{3}{2}(\mathcal{H}_0 - \hat{\mathcal{H}}_0)\beta)\boldsymbol{II}$	Part of the LH stress (B5), (B6)
$\boldsymbol{\eta}_{IM}^{\mathfrak{m}}$	$\frac{9M}{2}\beta^2 \boldsymbol{v} \nabla_{\mathsf{C}} \boldsymbol{V}$	Material immobility normal stress (B20)
$\boldsymbol{\eta}_0$	$-\frac{9\kappa}{4} \nabla_{\mathsf{C}}(\beta^2(\mathcal{H} - \hat{\mathcal{H}}_0 - \frac{3}{2}(\mathcal{H}_0 - \hat{\mathcal{H}}_0)\beta))$	Part of the LH normal stress (B5), (B6)
$\boldsymbol{\eta}_{\bar{\kappa}}$	$\frac{9\bar{\kappa}}{2}\beta(\mathcal{H}\boldsymbol{Id}_{\mathcal{S}} - \boldsymbol{II}) \nabla_{\mathsf{C}} \beta$	Part of the LH normal stress (B9)

Table 1. Quantities appearing in the fluid equation (3.4*a*). Here $\boldsymbol{V}_{\mathfrak{o}} \in T\mathbb{R}^3|_{\mathcal{S}}$ is the so-called observer velocity, which is arbitrary, not necessarily divergence free, and could be used as mesh velocity in a discretised problem for instance. Stress tensors $\tilde{\boldsymbol{\sigma}}$ are written modulo $\boldsymbol{Id}_{\mathcal{S}}$, respectively the resulting pressure gradient, in comparison to the listed references, since the model (3.4) is inextensible. The use of ∇_{C} on $T^0\mathcal{S}$ instead of ∇ is merely cosmetic; both are equivalent on scalar fields. Note that $\boldsymbol{\eta}_{IM}^{\mathfrak{m}}$ applies only within the material model.

Find the material velocity field $\boldsymbol{V} \in T\mathbb{R}^3|_{\mathcal{S}}$, scalar field $\beta \in T^0\mathcal{S}$ and generalised pressure field $\tilde{p} \in T^0\mathcal{S}$ such that

$$\rho\, \mathrm{D}_t^{\mathfrak{m}}\, \boldsymbol{V} = \mathrm{Grad}_{\mathsf{C}} \tilde{p} + \mathrm{Div}_{\mathsf{C}} \left(\tilde{\boldsymbol{\sigma}}_{NV} + \tilde{\boldsymbol{\sigma}}_1 + \tilde{\boldsymbol{\sigma}}_0 + \boldsymbol{v} \otimes \left(\delta_{\mathfrak{m}}^{\Phi} \boldsymbol{\eta}_{IM}^{\mathfrak{m}} + \boldsymbol{\eta}_0 + \boldsymbol{\eta}_{\bar{\kappa}} \right) \right), \tag{3.4a}$$

$$\left(M + \frac{\upsilon \xi^2}{2} \right) \dot{\beta} = \omega_1 + \omega_0 + \omega_{\bar{\kappa}} + \omega_{\mathrm{d}w}, \tag{3.4b}$$

$$\mathrm{Div}_{\mathsf{C}} \boldsymbol{V} = 0 \tag{3.4c}$$

holds for $\dot{\rho} = 0$ and given initial conditions for $\boldsymbol{V}$, β and mass density $\rho \in T^0\mathcal{S}$.

Quantities for the fluid equation (3.4*a*) are listed in table 1 and for the molecular equation (3.4*b*) in table 2. Material parameters can be found in table 3. Again the stress tensors are given modulo $\boldsymbol{Id}_{\mathcal{S}}$; the resulting pressure gradients are, respectively, incorporated into the generalised pressure $\tilde{p}$. Analogous to the surface Beris–Edwards model (3.1), activity, if additionally considered as in Nitschke & Voigt (2025*a*), has no effect, i.e. also the solutions of the hydrodynamic surface LH model exhibit a purely dissipative energy evolution as we can see in Appendix C. Many of the remarks made in § 3.1 remain valid in this context as well and are therefore not reiterated here, since (3.1) and (3.4) coincide for

$$\begin{aligned} a = \frac{2\hat{a}}{27}, \quad b = -\frac{2\hat{a}}{3} - 27\varpi, \quad c = \frac{2\hat{a}}{9} + \frac{27\varpi}{2}, \\ \mathcal{H}_0 = \hat{\mathcal{H}}_0 = 0, \quad \kappa = \bar{\kappa} = 2L. \end{aligned} \tag{3.5}$$

Again, we also formulate the model within a tangential calculus, including the use of covariant derivatives. For this purpose, we split the fluid equation (3.4*a*) into its projective

https://doi.org/10.1017/jfm.2026.11474 Published online by Cambridge University Press

Identifier	Expression	
$\dot{\beta}$	$\partial_t\beta + (\nabla_{\mathsf{C}}\beta)(\boldsymbol{V} - \boldsymbol{V}_{\mathfrak{o}})$	β rate (Nitschke & Voigt, 2023)
ω_1	$L\Delta_{\mathsf{C}}\beta$	Part of the mol. LH force (B4)
ω_0	$-\frac{3}{2}\kappa\beta(\mathcal{H} - \hat{\mathcal{H}}_0 - \frac{3}{2}(\mathcal{H}_0 - \hat{\mathcal{H}}_0)\beta)(\mathcal{H} - \hat{\mathcal{H}}_0 - 3(\mathcal{H}_0 - \hat{\mathcal{H}}_0)\beta)$	Part of the mol. LH force (B6)
$\omega_{\bar{\kappa}}$	$3\bar{\kappa}\mathcal{K}\beta$	Part of the mol. LH force (B10)
$\omega_{\mathrm{d}w}$	$-\frac{1}{6}\beta(\frac{2}{3} - \beta)(4\hat{a}(\frac{1}{3} - \beta) - 243\varpi\beta)$	Part of the mol. LH force (B11)

Table 2. Quantities appearing in the molecular equation (3.4*b*). Here $\boldsymbol{V}_{\mathfrak{o}} \in T\mathbb{R}^3|_{\mathcal{S}}$ is the so-called observer velocity, which is arbitrary, not necessarily divergence free, and could be used as mesh velocity in a discretised problem for instance. The use of componentwise operators ∇_{C}, Δ_{C} on $T^0\mathcal{S}$ instead of covariant ∇, Δ is merely cosmetic; both are equivalent on scalar fields.

Parameter	Domain	Name	Origin
υ	≥ 0	Isotropic viscosity	Aniso. viscous flux potential (B14)
ξ	$\in \mathbb{R}$	Anisotropy coefficient	Aniso. viscous flux potential (B14)
M	≥ 0	Immobility coefficient	Immobility flux potential (B19)
L	≥ 0	Elastic parameter	LH potential energy (4.25)
$\mathcal{H}_0$	$\in \mathbb{R}$	Spontaneous curvature at ordered state	LH potential energy (4.25)
$\hat{\mathcal{H}}_0$	$\in \mathbb{R}$	Spontaneous curvature at isotropic state	LH potential energy (4.25)
κ	≥ 0	Mean curvature-elastic moduli	LH potential energy (4.25)
$\bar{\kappa}$	$\in [0, \kappa]$	Gaussian curvature-elastic moduli	LH potential energy (4.25)
ϖ	See (A10)	Double-well parameter	LH potential energy (4.25)
$\hat{a}$	See (A10)	Double-well parameter	LH potential energy (4.25)

Table 3. Material parameters for the LH model (3.4). Given domains are only necessary, but not sufficient, for solvability or physical plausibility. For instance, Nitschke & Voigt (2025*b*) suggest $-3 < 2\xi < 3$ to maintain a positive definite lipid metric.

tangential and normal part, i.e.

$$\begin{aligned} \rho\boldsymbol{a} &= \nabla\bar{p} + \boldsymbol{f}_{NV} + \delta_{\mathfrak{m}}^{\Phi}\boldsymbol{f}_{IM}^{\mathfrak{m}} + \boldsymbol{f}_1 + \boldsymbol{f}_0 + \boldsymbol{f}_{\bar{\kappa}}, \\ \rho a_{\perp} &= \bar{p}\mathcal{H} + f_{NV}^{\perp} + \delta_{\mathfrak{m}}^{\Phi} f_{IM}^{\mathfrak{m},\perp} + f_1^{\perp} + f_0^{\perp} + f_{\bar{\kappa}}^{\perp}, \end{aligned} \tag{3.6}$$

where the tangential and normal fluid forces $\boldsymbol{f}_{NV}$, $f_{NV}^{\perp}$ (B17), $\boldsymbol{f}_{IM}^{\mathfrak{m}}$, $f_{IM}^{\mathfrak{m},\perp}$ (B21), $\boldsymbol{f}_1$, $f_1^{\perp}$ (B4), $\boldsymbol{f}_0$, $f_0^{\perp}$ (B5), (B6) and $\boldsymbol{f}_{\bar{\kappa}}$, $f_{\bar{\kappa}}^{\perp}$ (B10) are given in Appendix B. It should be noted that

$$\boldsymbol{f}_1 + \boldsymbol{f}_0 + \boldsymbol{f}_{\bar{\kappa}} = -\frac{3}{2}\left(\omega_1 + \omega_0 + \omega_{\bar{\kappa}}\right)\nabla\beta \tag{3.7}$$

holds, i.e. the tangential surface LH fluid force vanishes for constant β, as expected, since in this case the force is purely geometric and the associated normal force $f_1^{\perp} + f_0^{\perp} + f_{\bar{\kappa}}^{\perp}$

https://doi.org/10.1017/jfm.2026.11474 Published online by Cambridge University Press

reduces to a curvature-driven Helfrich force. Explicit representation of the tangential $\boldsymbol{a} = \boldsymbol{Id}_{\mathcal{S}}\, \mathrm{D}_t^{\mathfrak{m}}\, \boldsymbol{V}$ and normal acceleration $a_\perp = \boldsymbol{\nu}\, \mathrm{D}_t^{\mathfrak{m}}\, \boldsymbol{V}$ depending on an arbitrary observer frame can be found at the top of table 5, respectively (3.3). Even though this has no influence on the solution, the generalised pressure $\bar{p}$ is different here than in (3.4*a*). We have included in $\bar{p}$ only the forces arising from the double-well potential (B11) and the activity (B23), both of which reduce to pure pressure gradients. The molecular equation (3.4*b*) can essentially be used unchanged. In table 2 the subscript C may be omitted, as for scalar fields, the respective differential operators coincide with the covariant ones. Within the scalar rate $\dot{\beta}$ the relation $\boldsymbol{V} - \boldsymbol{V}_{\mathfrak{o}} = \boldsymbol{v} - \boldsymbol{v}_{\mathfrak{o}}$ already holds anyway, since all observers for the same moving surface have the same normal velocity. The inextensibility constraint (3.4*c*) becomes $\mathrm{div}\boldsymbol{v} = v_\perp \mathcal{H}$. The fully ordered case ($\beta = (2/3)$) leads to a surface Navier–Stokes–Helfrich model and is discussed in § 3.3.

3.3. *Surface Navier–Stokes–Helfrich models*

In the vicinity of the ordered equilibrium, we may assume that $\beta = (2/3)$. Incorporating this assumption into model (3.4), e.g. by means of a Lagrange multiplier formulation, eliminates the molecular equation (3.4*b*) and yields the surface Navier–Stokes–Helfrich model:

Find the material velocity field $\boldsymbol{V} \in T\mathbb{R}^3|_{\mathcal{S}}$ and generalised pressure field $\tilde{p} \in T^0\mathcal{S}$ such that

$$\rho\, \mathrm{D}_t^{\mathfrak{m}}\, \boldsymbol{V} = \mathrm{Grad}_{\mathsf{C}}\, \tilde{p} + \mathrm{Div}_{\mathsf{C}}\Big(\tilde{\upsilon}\, \Big(\boldsymbol{Id}_{\mathcal{S}} \nabla_{\mathsf{C}} \boldsymbol{V} + (\boldsymbol{Id}_{\mathcal{S}} \nabla_{\mathsf{C}} \boldsymbol{V})^T \Big) - \kappa\, (\mathcal{H} - \mathcal{H}_0)\, \boldsymbol{II} + \boldsymbol{\nu} \otimes \big(2M \delta_{\mathfrak{m}}^{\Phi} \boldsymbol{\nu} \nabla_{\mathsf{C}} \boldsymbol{V} - \kappa \nabla_{\mathsf{C}} \mathcal{H} \big) \Big), \tag{3.8a}$$

$$\mathrm{Div}_{\mathsf{C}}\, \boldsymbol{V} = 0 \tag{3.8b}$$

holds for $\dot{\rho} = 0$ and given initial conditions for $\boldsymbol{V}$ and mass density $\rho \in T^0\mathcal{S}$.

For $\mathcal{H}_0 = 0$, (3.8) also follows by assuming that $\beta = (2/3)$ in (3.1). Accordingly, the viscosity rescales as $\tilde{\upsilon} = \upsilon(1 + (\xi/3))^2$, although we may also simply set $\xi = 0$ without loss of generality, since the anisotropy coefficient no longer appears anywhere else, and thus, no actual anisotropic viscosity contributes to the solution. As expected, all Gaussian curvature-elastic terms vanish independently of $\bar{\kappa}$. It should be noted that if the assumption $\beta = (2/3)$ is justified by the fact that the immobility is small, i.e. $M \approx 0$, such that the molecular equation (3.4*b*) relaxes on a much faster time scale than the fluid equation (3.4*a*), then the immobility term in the fluid equation can obviously be neglected. In this case, the material ($\Phi = \mathfrak{m}$) and Jaumann ($\Phi = \mathcal{J}$) models are indistinguishable. Within the covariant differential calculus and the tangential-normal splitting of the fluid equations, the governing equations take the form

$$\rho \boldsymbol{a} = \nabla \bar{p} + \tilde{\upsilon} \left(\Delta \boldsymbol{v} + \mathcal{K} \boldsymbol{v} - 2 \left(\boldsymbol{II} - \frac{\mathcal{H}}{2} \boldsymbol{Id}_{\mathcal{S}} \right) \nabla v_\perp \right) + 2M \delta_{\mathfrak{m}}^{\Phi}\, (\mathcal{K} \boldsymbol{v} - \boldsymbol{II}\, (\nabla v_\perp + \mathcal{H} \boldsymbol{v})), \tag{3.9a}$$

$$\rho a_\perp = \mathcal{H} \bar{p} + 2\tilde{\upsilon} \Big(\boldsymbol{II} : \nabla \boldsymbol{v} - v_\perp \big(\mathcal{H}^2 - \mathcal{K} \big) \Big) + 2M \delta_{\mathfrak{m}}^{\Phi}\, (\Delta v_\perp + \boldsymbol{II} : \nabla \boldsymbol{v} + \nabla_{\boldsymbol{v}} \mathcal{H}) - \kappa \left(\Delta \mathcal{H} + \frac{1}{2} (\mathcal{H} - \mathcal{H}_0)\, (\mathcal{H}\, (\mathcal{H} + \mathcal{H}_0) - 4\mathcal{K}) \right), \tag{3.9b}$$

$$\mathrm{div}\boldsymbol{v} = \mathcal{H} v_\perp. \tag{3.9c}$$

The associated Jaumann model ($\Phi = \mathcal{J}$), respectively the neglected immobility ($M = 0$), is consistent with Reuther *et al.* (2020), Krause & Voigt (2023), Olshanskii (2023),

https://doi.org/10.1017/jfm.2026.11474 Published online by Cambridge University Press

Sischka *et al.* (2025), Sauer (2025) and with Arroyo & DeSimone (2009), Torres-Sánchez *et al.* (2019), Zhu *et al.* (2025) in the Stokes limit. We would like to emphasise once again that the material model ($\Phi = \mathfrak{m}$, $M > 0$) is, also in this setting, not invariant under rigid-body rotations. This lack of invariance may in fact be physically meaningful if a kind of rotational damping of the lipid molecules is assumed.

While the recovery of these known surface (Navier-)Stokes-Helfrich models for fluid deformable surfaces is appealing, their derivation differs. Brandner, Reusken & Schwering (2022) summarises different derivations of the surface Navier–Stokes equations. Their extensions towards (3.8) or (3.9) in Arroyo & DeSimone (2009), Torres-Sánchez *et al.* (2019), Reuther *et al.* (2020) always consider an *ad hoc* additional Helfrich energy. The derivations in § 4 do not require such an approach, the Helfrich terms naturally follow from the underlying surface liquid crystal models, similarly to the original derivation of Helfrich (1971).

4. Derivations

4.1. *The Q-tensor ansatz*

Essentially, we adopt a similar approach to that of Helfrich (1973). However, instead of considering a polar field normal to the surface $\mathcal{S}$ to describe a lipid bilayer, we employ an apolar field represented by an uniaxial Q-tensor field $\boldsymbol{Q} \in \mathcal{Q}^2\mathbb{R}^3|_{\mathcal{S}}$ with a normal eigenvector

$$\boldsymbol{Q} = S\left(\boldsymbol{\nu} \otimes \boldsymbol{\nu} - \frac{1}{3}\boldsymbol{Id}\right) = \beta\left(\boldsymbol{\nu} \otimes \boldsymbol{\nu} - \frac{1}{2}\boldsymbol{Id}_{\mathcal{S}}\right), \tag{4.1}$$

where $\boldsymbol{Id} = \boldsymbol{Id}_{\mathcal{S}} + \boldsymbol{\nu} \otimes \boldsymbol{\nu}$ is valid and $S = (3/2)\beta \in T^0\mathcal{S}$ is the scalar order field, respectively $\beta = (2/3)S \in T^0\mathcal{S}$ the eigenvalue field to the eigenvector field $\boldsymbol{\nu}$, i.e. it holds that $\boldsymbol{Q}\boldsymbol{\nu} = \beta\boldsymbol{\nu}$. With this ansatz, the lipid molecules are, on average, oriented orthogonally to the surface tangential planes and the amount of order is given by the scalar order S as the weighted average of the molecular orientation (Mottram & Newton 2014) deviating from $\boldsymbol{\nu}$. For convenience, we use β instead of S in this paper. Note that $\boldsymbol{Q}$ in (4.1) is surface conforming without any flat-degenerated part; see Nitschke & Voigt (2025*b*).

The advantage of modelling lipid layers as Q-tensor fields lies in the ability to describe molecular alignment as being, on average, normal to the surface, while also incorporating an additional degree of freedom for the statistical order. This approach allows us to build on established surface Beris–Edwards models to develop hydrodynamic descriptions of lipid bilayers, as discussed in § 4.2. A limitation of (4.1), however, is that it is an apolar ansatz, i.e. due to head–tail symmetry of the molecules we can only represent symmetric lipid bilayers *a priori*. The symmetry break required to obtain asymmetric lipid bilayers must occur elsewhere in the process. This is addressed in § 4.3.

4.2. *Surface Beris–Edwards model for symmetric lipid bilayers*

In this section we use the surface-conforming Beris–Edwards models in Nitschke & Voigt (2025*b*) as a starting point and incorporate a suitable constraint providing the ansatz (4.1). Since ansatz (4.1) as well as the surface-conforming models comprise up–down symmetry, i.e. the exterior and interior of the surface are indistinguishable in any way, we could only describe symmetric lipid bilayers, see figure 1, without introducing any additional symmetry-breaking mechanism. For the reader's convenience, a summary of the surface Beris–Edwards model from Nitschke & Voigt (2025*b*) together with the active terms introduced in Nitschke & Voigt (2025*a*) are given in Appendix D.

https://doi.org/10.1017/jfm.2026.11474 Published online by Cambridge University Press

A reasonable orthogonal decomposition of $\boldsymbol{Q} \in \mathcal{Q}^2\mathbb{R}^3|_{\mathcal{S}}$ is provided by

$$\boldsymbol{Q} = \boldsymbol{q} + \boldsymbol{\eta} \otimes \boldsymbol{\nu} + \boldsymbol{\nu} \otimes \boldsymbol{\eta} + \beta \left(\boldsymbol{\nu} \otimes \boldsymbol{\nu} - \frac{1}{2} \boldsymbol{Id}_{\mathcal{S}} \right), \tag{4.2}$$

where $\boldsymbol{q} \in \mathcal{Q}^2\mathcal{S}$ yields the flat-degenerated part, $\boldsymbol{\eta} \in T\mathcal{S}$ the surface non-conforming part and $\beta \in T^0\mathcal{S}$ the uniaxial normal part. The surface-conforming constraint $\boldsymbol{\eta} = \boldsymbol{0}$ is already incorporated in the surface-conforming Beris–Edwards model (D1). Therefore, we only need to consider a 'no flat degeneracy' ($\boldsymbol{q} = \boldsymbol{0}$) constraint for our purpose. We account for possible constraint forces in Appendix E and conclude that it suffices to omit the flat-degenerated molecular equation (D1*c*) and simply substitute $\boldsymbol{q} = \boldsymbol{0}$ throughout the remaining model.

We first address the elastic contributions arising from the elastic energy functional

$$\mathfrak{U}_{EL} = \frac{L}{2} \| \nabla_{\mathsf{C}} \boldsymbol{Q} \|^2_{\mathrm{L}^2(T^3\mathbb{R}^3|_{\mathcal{S}})}. \tag{4.3}$$

The relevant terms in table 5 yield

$$\begin{aligned}
\boldsymbol{\sigma}_{EL} &= -\frac{3}{2} L \left(\nabla\beta \otimes \nabla\beta - \frac{\|\nabla\beta\|^2}{2} \boldsymbol{Id}_{\mathcal{S}} + 3\mathcal{H}\beta^2 \left(\boldsymbol{II} - \frac{\mathcal{H}}{2} \boldsymbol{Id}_{\mathcal{S}} \right) \right), \\
\boldsymbol{\zeta}_{EL} &= -\frac{3}{2} L (2\boldsymbol{II}\nabla\beta + \beta\nabla\mathcal{H}), \\
\omega_{EL} &= L \Big(\Delta\beta - 3\beta \big(\mathcal{H}^2 - 2\mathcal{K} \big) \Big).
\end{aligned} \tag{4.4}$$

Note that the tangential elastic fluid force $\mathrm{div}\boldsymbol{\sigma}_{EL}$ combined with the elastic part of the tangential surface-conforming constraint force $-3\beta\boldsymbol{II}\boldsymbol{\zeta}_{EL}$ results in

$$\begin{aligned}
&\mathrm{div}\boldsymbol{\sigma}_{EL} - 3\beta\boldsymbol{II}\boldsymbol{\zeta}_{EL} \\
&= -\frac{3}{2} L \Big(\Delta\beta\nabla\beta + \nabla^2\beta\nabla\beta - \nabla^2\beta\nabla\beta + 3\beta^2 \left(\boldsymbol{II}\nabla\mathcal{H} - \frac{\mathcal{H}}{2}\nabla\mathcal{H} \right) \\
&\quad + 6\mathcal{H}\beta \left(\boldsymbol{II}\nabla\beta - \frac{\mathcal{H}}{2}\nabla\beta \right) + \frac{3}{2}\mathcal{H}\beta^2\nabla\mathcal{H} - 3\beta \left(2\mathcal{H}\boldsymbol{II}\nabla\beta - 2\mathcal{K}\nabla\beta + \beta\boldsymbol{II}\nabla\mathcal{H} \right) \Big) \\
&= -\frac{3}{2} L \left(\Delta\beta - 3\beta \big(\mathcal{H}^2 - 2\mathcal{K} \big) \right) \nabla\beta = -\frac{3}{2} \omega_{EL} \nabla\beta,
\end{aligned} \tag{4.5}$$

since $\mathrm{div}\boldsymbol{II} = \nabla\mathcal{H}$ and $\boldsymbol{II}^2 = \mathcal{H}\boldsymbol{II} - \mathcal{K}\boldsymbol{Id}_{\mathcal{S}}$ is valid. The normal elastic fluid force $\boldsymbol{II} : \boldsymbol{\sigma}_{EL}$ combined with the elastic part of the normal surface-conforming constraint force $3\mathrm{div}(\beta\boldsymbol{\zeta}_{EL})$ becomes

$$\begin{aligned}
\boldsymbol{II} : \boldsymbol{\sigma}_{EL} + 3\mathrm{div}(\beta\boldsymbol{\zeta}_{EL}) = -\frac{3}{4} L \Big(&14\nabla\beta\boldsymbol{II}\nabla\beta - \mathcal{H} \|\nabla\beta\|^2 \\
&+ 3\beta \left(4\boldsymbol{II} : \nabla^2\beta + 8\nabla\mathcal{H}\nabla\beta + \beta \left(2\Delta\mathcal{H} + \mathcal{H}(\mathcal{H}^2 - 4\mathcal{K}) \right) \right) \Big).
\end{aligned} \tag{4.6}$$

This implies that elasticity of symmetric lipid bilayers already comprises the bending force $f^{\perp}_{BE}\boldsymbol{\nu}$ for surfaces with up–down symmetry and mean curvature-elastic moduli $\kappa = (9/2)L\beta^2$. Since the lipid molecules already define the surface geometry, we omit the lipid-independent bending force $f^{\perp}_{BE}$ and retain only the one arising from the elasticity in

https://doi.org/10.1017/jfm.2026.11474 Published online by Cambridge University Press

terms of the scalar order parameter. The molecular thermotropic force results in

$$\omega_{TH} = -\big(2a + b\beta + 3c\beta^2\big)\beta. \tag{4.7}$$

Other thermotropic contributions have no influence on the model. The immobility terms yield

$$\boldsymbol{\sigma}^{\Phi}_{IM} = \mathbf{0}, \qquad \boldsymbol{\zeta}^{\Phi}_{IM} = \begin{cases} \mathbf{0} & \text{for } \Phi = \mathcal{J}, \\ \dfrac{3}{2} M\beta\,(\boldsymbol{\nabla} v_\perp + \boldsymbol{II}\,\boldsymbol{v}) & \text{for } \Phi = \mathfrak{m}; \end{cases} \tag{4.8}$$

see (B21) for the corresponding fluid forces. Nematic viscosity terms become

$$\boldsymbol{\sigma}^0_{NV} + \xi\boldsymbol{\sigma}^1_{NV} + \xi^2\boldsymbol{\sigma}^2_{NV} = \tilde{\boldsymbol{\sigma}}_{NV} + \frac{\upsilon\xi}{2}\dot{\beta}\left(1 + \frac{\xi\beta}{2}\right)\boldsymbol{Id}_{\mathcal{S}}, \qquad \widetilde{\omega}^2_{NV} = 0. \tag{4.9}$$

Due to inextensibility, we only have to consider

$$\tilde{\boldsymbol{\sigma}}_{NV} = \upsilon\left(1 - \frac{\xi\beta}{2}\right)^2\big(\boldsymbol{\nabla}\boldsymbol{v} + \boldsymbol{\nabla}^T\boldsymbol{v} - 2v_\perp\boldsymbol{II}\big); \tag{4.10}$$

see (B17) for the corresponding fluid forces. Nematic activity does not contribute in a inextensible media, i.e.

$$\boldsymbol{\sigma}_{NA} = \mathbf{0}. \tag{4.11}$$

Nevertheless, even though it does not affect the inextensible model, we note the presence of an active pressure $p_{AC} = \alpha_{IA} - (\alpha_{NA}/2)\beta$, comprising a nematic part controlled by parameter $\alpha_{NA} \in \mathbb{R}$ and a geometric part controlled by the parameter $\alpha_{IA} \in \mathbb{R}$; see Nitschke & Voigt (2025*a*). The corresponding pressure force therefore reads

$$\begin{aligned} \boldsymbol{F}_{AC} &= \mathrm{Div}_{\mathsf{C}}\left(\left(\alpha_{IA} - \frac{\alpha_{NA}}{2}\beta\right)\boldsymbol{Id}_{\mathcal{S}}\right) = \alpha_{IA}\mathrm{Grad}_{\mathsf{C}}1 - \frac{\alpha_{NA}}{2}\mathrm{Grad}_{\mathsf{C}}\beta \\ &= -\frac{\alpha_{NA}}{2}\boldsymbol{\nabla}\beta + \left(\alpha_{IA} - \frac{\alpha_{NA}}{2}\beta\right)\mathcal{H}\boldsymbol{v}. \end{aligned} \tag{4.12}$$

Eventually, the surface Beris–Edwards model (D1), the 'no flat degeneracy' constraint, and rewriting all relevant terms in the $\mathbb{R}^3$ calculus, yield the model (3.1) for symmetric lipid bilayers.

4.3. *Hydrodynamic surface LH model for asymmetric lipid bilayers*

In this section we derive the surface LH energy as a special case of a polarised surface Landau–De Gennes energy, which consists of a nematic elastic contribution, a thermotropic contribution, similar to Nitschke *et al.* (2018, 2020) and an up–down symmetry-breaking mechanism. The reduction to the lipid-molecule level is carried out using the ansatz (4.1). For this purpose, we identify all invariants for asymmetric lipid bilayers up to a certain order, similar to the procedure in Helfrich (1973) and Alexe-Ionescu (1993). We then reformulate these into a form analogous to the Helfrich energy, which generalises it accordingly. The governing equations derived from this formulation and the Lagrange–D'Alembert principle for moving surfaces (Nitschke & Voigt 2025*b*) are provided in Appendix B.

The componentwise surface derivative of (4.1) results in

$$\boldsymbol{\nabla}_{\mathsf{C}}\boldsymbol{Q} = \left(\boldsymbol{v}\otimes\boldsymbol{v} - \frac{1}{2}\boldsymbol{Id}_{\mathcal{S}}\right)\otimes\boldsymbol{\nabla}\beta - \frac{3}{2}\beta\left(\boldsymbol{v}\otimes\boldsymbol{II} + (\boldsymbol{v}\otimes\boldsymbol{II})^{T_{(1\,2)}}\right), \tag{4.13}$$

https://doi.org/10.1017/jfm.2026.11474 Published online by Cambridge University Press

where $[(\boldsymbol{\nu}\otimes\boldsymbol{II})^{T_{(1\,2)}}]_{ABC}=\nu_B II_{AC}$ in arbitrary Euclidean coordinates. Both summands and all their transpositions are mutual orthogonal or symmetric, i.e. all scalar-valued quadratic invariants of (4.13) are given by $\|\nabla\beta\|^2_{T\mathcal{S}}$ and $\|\beta\boldsymbol{II}\|^2_{T^2\mathcal{S}}=(\mathcal{H}^2-2\mathcal{K})\beta^2$ or $(\mathrm{Tr}\boldsymbol{II})^2\beta^2=\mathcal{H}^2\beta^2$. Therefore, we could reduce the quadratic energy approach

$$\int_{\mathcal{S}} l_{A_1,A_2,A_3,B_1,B_2,B_3}[\nabla_{\mathsf{C}}\boldsymbol{Q}]^{A_1,A_2,A_3}[\nabla_{\mathsf{C}}\boldsymbol{Q}]^{B_1,B_2,B_3}\mathrm{d}\mathcal{S} \tag{4.14}$$

to the elastic energy potential

$$\tilde{\mathfrak{U}}_{el}:=\frac{l_1}{2}\,\|\nabla\beta\|^2_{\mathrm{L}(T\mathcal{S})}+\frac{l_0}{2}\,\|\mathcal{H}\beta\|^2_{\mathrm{L}^2(T^0\mathcal{S})}-\bar{l}_0\int_{\mathcal{S}}\mathcal{K}\beta^2\mathrm{d}\mathcal{S} \tag{4.15}$$

with material parameters $l_1\geq 0$ and $l_0\geq\bar{l}_0\geq 0$. For instance, if we substitute ansatz (4.1) into the one-constant elastic energy potential (4.3), we obtain

$$\mathfrak{U}_{EL}=\frac{3}{4}L\left(\|\nabla\beta\|^2_{\mathrm{L}^2(T\mathcal{S})}+3\,\|\mathcal{H}\beta\|^2_{\mathrm{L}^2(T^0\mathcal{S})}-6\int_{\mathcal{S}}\mathcal{K}\beta^2\mathrm{d}\mathcal{S}\right), \tag{4.16}$$

i.e. the parameter relation would be $l_1=3L/2$ and $l_0=\bar{l}_0=9L/2$. Other conceivable elastic energy potentials that are quadratic in $\boldsymbol{Q}$ – for instance, those involving the commonly used elastic parameters $L_1=L, L_2, L_3$ (Mori *et al.* 1999; Mottram & Newton 2014) – yield energies with different proportions. (If we consider a constant extension in the normal direction of $\boldsymbol{Q}$, cf. Nitschke *et al.* (2018), we obtain $(L_2/2)\|\mathrm{Div}_{\mathsf{C}}\boldsymbol{Q}\|^2_{\mathrm{L}^2(T\mathbb{R}^3|_{\mathcal{S}})}=(L_2/8)(\|\nabla\beta\|^2_{\mathrm{L}^2(T\mathcal{S})}+9\|\beta\mathcal{H}\|^2_{\mathrm{L}^2(T^0\mathcal{S})})$ and $(L_3/2)\langle\nabla_{\mathsf{C}}\boldsymbol{Q},\nabla^T_{\mathsf{C}}\boldsymbol{Q}\rangle_{\mathrm{L}^2(T^3\mathbb{R}^3|_{\mathcal{S}})}=(L_3/8)(\|\nabla\beta\|^2_{\mathrm{L}^2(T\mathcal{S})}+9\|\beta\mathcal{H}\|^2_{\mathrm{L}^2(T^0\mathcal{S})}-18\int_{\mathcal{S}}\mathcal{K}\mathrm{d}\mathcal{S})$ for instance.) Note that (4.15) states Helfrich's bending energy (Helfrich 1973) for constant β and neglected spontaneous curvature, where the curvature-elastic moduli yield $\kappa=l_0\beta^2$ and $\bar{\kappa}=\bar{l}_0\beta^2$.

In order to also incorporate spontaneous curvature effects we have to break the up–down symmetry of our approach. The elastic potential (4.15) cannot accomplish this on its own. In the field of liquid crystals, such a polarisation has already been derived via the piezoelectric effect (Meyer 1969; Helfrich 1971). Essentially, this involves assuming an asymmetry in the physics of the nematic phase, which exhibits either splay and/or bend structures. Lipid bilayers, with average molecule directions perpendicular to the surface, may likewise exhibit a splay, since parallel alignment cannot be sustained on a curved surface, cf. figure 2, but no bending asymmetry, which would require molecules to possess, on average, a tangential component. Such a splay asymmetry can originate from a variety of mechanisms (Zimmerberg & Kozlov 2005), for instance, if the inner layer consists of a different molecular composition than the outer one (London 2019; Lorent *et al.* 2020; Bogdanov *et al.* 2020; Enoki & Heberle 2023), if the molecular density differs between the two sides (Różycki & Lipowsky 2015; Sreekumari & Lipowsky 2018; Ghosh *et al.* 2019; Sreekumari & Lipowsky 2022; Lipowsky *et al.* 2023), or if binding of proteins, such as coat or scaffolds proteins, is included (Hu, Zhang & Weinan 2007; Kirchhausen 2012; Saleem *et al.* 2015; Kahraman, Langen & Haselwandter 2018; Mironov *et al.* 2020). This does not violate the apolarity of the average lipid orientations in the normal direction, but rather pertains to the physical conditions that a bilayer might inherently possess. In Govers & Vertogen (1984), Barbero *et al.* (1986), Alexe-Ionescu (1993), Mottram & Newton (2014) flexoelectric polarisation in terms of Q tensors is already discussed. Considering the normal direction $\boldsymbol{\nu}$ as the polarisation direction yields

https://doi.org/10.1017/jfm.2026.11474 Published online by Cambridge University Press

$$\boldsymbol{\nu}\mathrm{Div}_{\mathrm{C}}\,\boldsymbol{Q}=-\frac{3}{2}\mathcal{H}\beta,\qquad \boldsymbol{\nu}(\nabla_{\mathrm{C}}\,\boldsymbol{Q}):\boldsymbol{Q}=\frac{3}{4}\mathcal{H}\beta^2,\qquad \boldsymbol{\nu}\,\boldsymbol{Q}\mathrm{Div}_{\mathrm{C}}\,\boldsymbol{Q}=-\frac{3}{2}\mathcal{H}\beta^2, \tag{4.17}$$

for the non-vanishing (E_1, E_5, E_6) terms in Alexe-Ionescu (1993). As we see below, the thermotropic potential is a fourth-order polynomial in β and $\mathcal{H}$, albeit with vanishing coefficients for the mean curvature. Therefore, we extend the expansion of the polarisation up to third order, which, additionally, comprises the non-vanishing terms

$$\begin{aligned}\boldsymbol{\nu}\,\boldsymbol{Q}(\nabla_{\mathrm{C}}\,\boldsymbol{Q}):\boldsymbol{Q}&=\frac{3}{4}\mathcal{H}\beta^3, & (\mathrm{Tr}\,\boldsymbol{Q}^2)\boldsymbol{\nu}\mathrm{Div}_{\mathrm{C}}\,\boldsymbol{Q}&=-\frac{9}{4}\mathcal{H}\beta^3,\\ \boldsymbol{\nu}(\nabla_{\mathrm{C}}\,\boldsymbol{Q}):\boldsymbol{Q}^2&=-\frac{3}{8}\mathcal{H}\beta^3, & \boldsymbol{\nu}\,\boldsymbol{Q}^2\mathrm{Div}_{\mathrm{C}}\,\boldsymbol{Q}&=-\frac{3}{2}\mathcal{H}\beta^3.\end{aligned} \tag{4.18}$$

Therefore, the polarised elastic energy, up to forth polynomial order, respectively third order in β, is of the form

$$\int_{\mathcal{S}}\left(k_1+\frac{k_2}{2}\beta+\frac{k_3}{3}\beta^2\right)\mathcal{H}\beta\,\mathrm{d}\mathcal{S}, \tag{4.19}$$

where $k_1, k_2, k_3\in\mathbb{R}$ are the polarisation parameters. Order polarisation in terms of $\nabla\beta$ is not included as a consequence. Eventually, we approach the polarised elastic energy by

$$\mathfrak{U}_{el}:=\frac{l_1}{2}\,\|\nabla\beta\|^2_{\mathrm{L}^2(T\mathcal{S})}+\int_{\mathcal{S}}\frac{l_0}{2}\mathcal{H}^2\beta^2-\bar{l}_0\mathcal{K}\beta^2+\frac{k_3}{3}\mathcal{H}\beta^3+\frac{k_2}{2}\mathcal{H}\beta^2+k_1\mathcal{H}\beta\mathrm{d}\mathcal{S}. \tag{4.20}$$

Using (4.1) the thermotropic energy becomes

$$\begin{aligned}\mathfrak{U}_{TH}&=\int_{\mathcal{S}}a\mathrm{Tr}\,\boldsymbol{Q}^2+\frac{2b}{3}\mathrm{Tr}\,\boldsymbol{Q}^3+c\mathrm{Tr}\,\boldsymbol{Q}^4\mathrm{d}\mathcal{S}\\ &=\int_{\mathcal{S}}\frac{3a}{2}\beta^2+\frac{b}{2}\beta^3+\frac{9c}{8}\beta^4\mathrm{d}\mathcal{S}=\int_{\mathcal{S}}\frac{A}{2}\beta^2+\frac{B}{3}\beta^3+\frac{C}{4}\beta^4\mathrm{d}\mathcal{S},\end{aligned} \tag{4.21}$$

i.e. $A=3a$, $B=3b/2$ and $C=9c/2$ holds for the thermotropic coefficients. Due to the zeroth-order derivative terms, the elastic and thermotropic energy should not be considered separately. The polarised surface Landau–de Gennes energy now reads

$$\begin{aligned}\mathfrak{U}_{LdG}&:=\mathfrak{U}_{el}+\mathfrak{U}_{TH}\\ &=\frac{l_1}{2}\,\|\nabla\beta\|^2_{\mathrm{L}^2(T\mathcal{S})}\\ &\quad+\int_{\mathcal{S}}k_1\mathcal{H}\beta+\frac{A+k_2\mathcal{H}+l_0\mathcal{H}^2-2\bar{l}_0\mathcal{K}}{2}\beta^2+\frac{B+k_3\mathcal{H}}{3}\beta^3+\frac{C}{4}\beta^4\mathrm{d}\mathcal{S}.\end{aligned} \tag{4.22}$$

Note that this potential has a minimum for $l_1\geq 0$, $l_0\geq\bar{l}_0\geq 0$, $C>0$ and $k_3\in(-(3/2)\sqrt{C(2l_0-\bar{l}_0)},(3/2)\sqrt{C(2l_0-\bar{l}_0)})$ (A8), see Appendix A.

The material parameters in (4.22) appear to be somewhat unintuitive, as they represent purely formal expansion parameters. Therefore, we aim to reformulate (4.22) in the form

$$\mathfrak{U}_{LH}:=\frac{3L}{4}\,\|\nabla\beta\|^2_{\mathrm{L}^2(T\mathcal{S})}+\int_{\mathcal{S}}\frac{f_\kappa(\beta)}{2}\big(\mathcal{H}-f_{\mathcal{H}_0,\hat{\mathcal{H}}_0}(\beta)\big)^2-f_{\bar{\kappa}}(\beta)\mathcal{K}+f_{\varpi,\hat{a}}(\beta)\mathrm{d}\mathcal{S}, \tag{4.23}$$

such that f_κ, $f_{\mathcal{H}_0,\hat{\mathcal{H}}_0}$, $f_{\bar{\kappa}}$ and $f_{\varpi,\hat{a}}$ are polynomials in β, (4.22) is satisfied as generally as possible and $f_\kappa((2/3))=\kappa$, $f_{\mathcal{H}_0,\hat{\mathcal{H}}_0}((2/3))=\mathcal{H}_0$, $f_{\bar{\kappa}}((2/3))=\bar{\kappa}$, and $f_{\varpi,\hat{a}}((2/3))=-\varpi$ (local minimum) hold at the fully ordered state. By providing a sufficient polynomial ansatz, incorporating the required conditions and comparing coefficients, we obtain the

https://doi.org/10.1017/jfm.2026.11474 Published online by Cambridge University Press

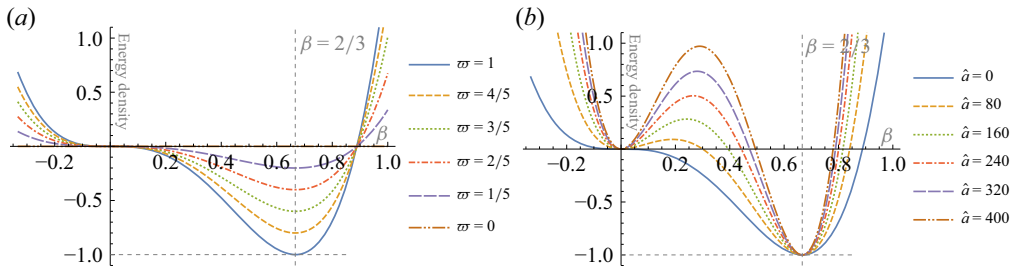


Figure 3. Energy density plots of the double-well potential (4.24). In (*a*) we stipulate $\hat{a} = 0$ and choose some values for ϖ. Their additive inverse equal the minimum values at the fully ordered state $\beta = (2/3)$. In (*b*) we use $\varpi = 1$ and specify some values for $\hat{a}$. Only $\hat{a} = 0$ yields an inflection point at the isotropic state $\beta = 0$ instead of a minimum for $\hat{a} > 0$.

quadratic curvature-elastic polynomials $f_\kappa(\beta) = (9/4)\kappa\beta^2$ and $f_{\bar\kappa}(\beta) = (9/4)\bar\kappa\beta^2$, linear spontaneous curvature polynomial $f_{\mathcal{H}_0,\hat{\mathcal{H}}_0}(\beta) = \hat{\mathcal{H}}_0 + (3/2)(\mathcal{H}_0 - \hat{\mathcal{H}}_0)\beta$ and double-well potential

$$f_{\varpi,\hat{a}}(\beta) = \frac{9}{4}\beta^2\left(\frac{\hat{a}}{9}\left(\frac{2}{3}-\beta\right)^2 - \frac{3\varpi}{2}\beta\left(4-\frac{9}{2}\beta\right)\right); \tag{4.24}$$

see figure 3. Similar linear spontaneous curvature polynomials have been considered to interpolate between spontaneous curvature values for coexisting, e.g. liquid-ordered and liquid-disordered, phases (Seifert 1993; Taniguchi 1996; Bachini *et al.* 2023*a*; Sischka & Voigt 2025).

As a consequence, the polarised surface Landau–de Gennes energy becomes

$$\begin{aligned}\mathfrak{U}_{LH} = {}& \frac{3}{4}L\,\|\nabla\beta\|^2_{\mathrm{L}^2(T\mathcal{S})} \\ & + \int_{\mathcal{S}} \frac{9}{4}\beta^2\left(\frac{\kappa}{2}\left(\mathcal{H} - \left(\hat{\mathcal{H}}_0 + \frac{3}{2}(\mathcal{H}_0 - \hat{\mathcal{H}}_0)\beta\right)\right)^2 - \bar\kappa\mathcal{K}\right) + f_{\varpi,\hat{a}}(\beta)\,\mathrm{d}\mathcal{S},\end{aligned} \tag{4.25}$$

and we name it surface LH energy. Alternative approaches beyond this resulting linear interpolation of the spontaneous curvature with respect to a scalar order are conceivable; see, e.g. Bartels *et al.* (2012). Note that the surface LH energy (4.25) involves only seven material parameters (listed in table 3), instead of nine as in the polarised surface Landau–de Gennes energy (4.22). Its material parameters are uniquely determined as follows:

$$\begin{aligned} A &= \frac{9\kappa}{4}\hat{\mathcal{H}}_0^2 + \frac{2}{9}\hat{a}, & k_1 &= 0, & l_0 &= \frac{9\kappa}{4}, \\ B &= \frac{81\kappa}{8}(\mathcal{H}_0 - \hat{\mathcal{H}}_0)\hat{\mathcal{H}}_0 - \frac{2\hat{a}+81\varpi}{2}, & k_2 &= -\frac{9\kappa}{2}\hat{\mathcal{H}}_0, & \bar{l}_0 &= \frac{9\bar\kappa}{4}, \\ C &= \frac{81\kappa}{8}(\mathcal{H}_0 - \hat{\mathcal{H}}_0)^2 + \frac{4\hat{a}+243\varpi}{4}, & k_3 &= -\frac{81\kappa}{8}(\mathcal{H}_0 - \hat{\mathcal{H}}_0), & l_1 &= \frac{3L}{2}. \end{aligned} \tag{4.26}$$

The restriction of k_3 yields now the restriction (A10) of the double-well parameter $\hat{a}$ and ϖ; see Appendix A. It should be noted that the $C = 0$ case is included here, although not discussed in Appendix A. Nevertheless, this yields $\mathcal{H}_0 = \hat{\mathcal{H}}_0$ and $\hat{a} = \varpi = 0$, and thus,

https://doi.org/10.1017/jfm.2026.11474 Published online by Cambridge University Press

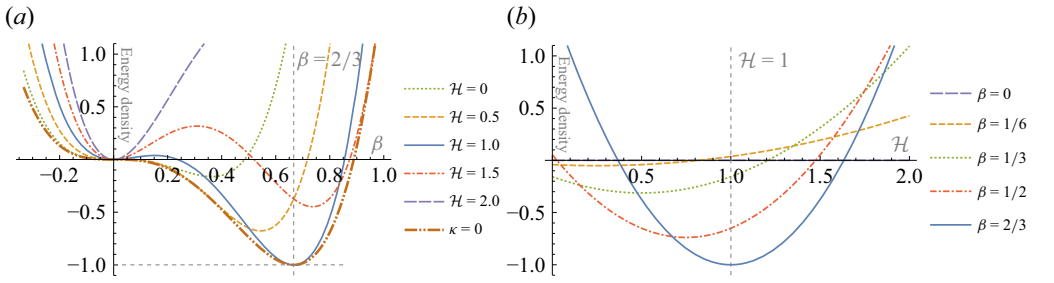


Figure 4. Energy density plots of the energy (4.28) ($\hat{\mathcal{H}}_0 = \hat{a} = 0$) with $L = \bar{\kappa} = 0$. We stipulate $\kappa = 5$ and $\mathcal{H}_0 = \varpi = 1$. In panel ($a$) we fix the mean curvature $\mathcal{H}$ for some fixed values around $\mathcal{H}_0 = 1$. Additional we add the $\kappa = 0$ case, which does not depend on $\mathcal{H}$ and leads β to the fully ordered state $\beta = (2/3)$. Panel (b) shows the dependency with respect to $\mathcal{H}$ for some fixed βs.

$$\mathfrak{U}_{LH}|_{\mathcal{H}_0=\hat{\mathcal{H}}_0,\hat{a}=0} = \frac{3}{4}L\,\|\nabla\beta\|^2_{\mathrm{L}^2(T\mathcal{S})} + \int_{\mathcal{S}} \frac{9}{4}\beta^2\left(\frac{\kappa}{2}\left(\mathcal{H}-\mathcal{H}_0\right)^2 - \bar{\kappa}\mathcal{K} - \frac{3\varpi}{2}\beta\left(4-\frac{9}{2}\beta\right)\right)\mathrm{d}\mathcal{S}, \tag{4.27}$$

which remains bounded below even for $\varpi = 0$. The special case (4.27) essentially states that the spontaneous curvature $\mathcal{H}_0 = \hat{\mathcal{H}}_0$ does not depend on the scale order β, and that the isotropic state ($\beta \equiv 0$) is possible but not stable due to $\hat{a} = 0$. By contrast, another special case occurs when no spontaneous curvature $\hat{\mathcal{H}}_0 = 0$ is present in the isotropic state, i.e.

$$\mathfrak{U}_{LH}|_{\hat{\mathcal{H}}_0=0,\hat{a}=0} = \frac{3}{4}L\,\|\nabla\beta\|^2_{\mathrm{L}^2(T\mathcal{S})} + \int_{\mathcal{S}} \frac{9}{4}\beta^2\left(\frac{\kappa}{2}\left(\mathcal{H}-\frac{3}{2}\mathcal{H}_0\beta\right)^2 - \bar{\kappa}\mathcal{K} - \frac{3\varpi}{2}\beta\left(4-\frac{9}{2}\beta\right)\right)\mathrm{d}\mathcal{S}; \tag{4.28}$$

see figure 4. It should be noted that $\hat{\mathcal{H}}_0$ and $\hat{a}$ become increasingly insignificant near the ordered state ($\beta \approx (2/3)$) anyway.

The converse of material parameter relation (4.26) is not uniquely determined, due to the reduction of the amount of parameters. In table 4 we give an overview of these possible relations for the two special cases above. However, in order to address phase coexistence and account for the different properties of the liquid-ordered and liquid-disordered phases, as in Baumgart *et al.* (2003), these special cases are not sufficient and the full set of parameters, allowing for $\mathcal{H}_0 \neq \hat{\mathcal{H}}_0$, are required.

It should also be noted that the fully ordered regime ($\beta = (2/3)$) yields the common Helfrich energy

$$\mathfrak{U}_{LH}|_{\beta\equiv\frac{2}{3}} = \int_{\mathcal{S}} \frac{\kappa}{2}\left(\mathcal{H}-\mathcal{H}_0\right)^2 - \bar{\kappa}\mathcal{K} - \varpi\,\mathrm{d}\mathcal{S} \tag{4.29}$$

with a constant offset ($-\varpi$), which has not any impact on variations for inextensible materials.

The derivation of the governing equations from the LH energy (4.25) and additional dynamical contributions, such as linear momentum and viscous forces, is carried out directly via the Lagrange–d'Alembert principle in Appendix B.

https://doi.org/10.1017/jfm.2026.11474 Published online by Cambridge University Press

Assumptions:	$\hat{\mathcal{H}}_0 = \mathcal{H}_0$		$\hat{\mathcal{H}}_0 = 0$
		$\hat{a} = 0$	
Constraints:	$k_3 = 0$		$k_2 = 0$
	$2C + 3B = 0$		$A = 0$
	$k_2^2 = 4l_0 A$		$4k_3^2 = 9l_0(2C + 3B)$
		$k_1 = 0$	
Relations:	$\mathcal{H}_0 = -\dfrac{k_2}{2l_0}$		$\mathcal{H}_0 = -\dfrac{2k_3}{9l_0}$
		$L = \dfrac{2}{3}l_1$	
		$\kappa = \dfrac{4}{9}l_0$	
		$\bar{\kappa} = \dfrac{4}{9}\bar{l}_0$	
		$\varpi = -\dfrac{2}{81}B$	

Table 4. Inverse of material parameter relations (4.26) for the special cases (4.27) (left column) and (4.28) (right column). The middle column holds for both cases. Since the number of material parameters is reduced from 9 to 5, four constraints on the parameters follow. The relations are not unique due to some of these constraints.

5. Discussion

We have derived various hydrodynamic liquid crystal models for lipid bilayers. They include a hydrodynamic surface LH model for asymmetric lipid bilayers and a surface Beris–Edwards model for symmetric lipid bilayers. The latter directly follows from the surface-conforming Beris–Edwards model derived in Nitschke & Voigt (2025*b*) considering an additional 'no flat degeneracy' constraint. It is also a special case of the (LH) model if the polarisation vanishes. The (LH) model builds on a special case of a surface polarised Landau–de Gennes energy and is derived using the Lagrange–d'Alembert principle. Both models consider a scalar order parameter that quantifies the degree of the molecular alignment along the surface normal. This order determines the bending properties, it influences the surface hydrodynamics and, in case of the hydrodynamic surface LH model, it introduces curvature-order coupling that breaks up–down symmetry. For the fully ordered state, the equations reduce to the surface (Navier–)Stokes–Helfrich model for fluid deformable surfaces (Arroyo & DeSimone 2009; Torres-Sánchez *et al.* 2019; Reuther *et al.* 2020) and in its overdamped limit to the classical Helfrich model with a local inextensibility constraint. The results therefore also provide an alternative derivation of the surface (Navier–)Stokes–Helfrich model or even the classical Helfrich model. However, the main contributions are the derived hydrodynamic liquid crystal models for lipid bilayers in (3.1) and (3.4) for symmetric and asymmetric cases, respectively. In order to demonstrate the potential impact of the molecular order on the dynamics of these highly coupled systems, we explore numerical simulations. Details on the numerical approach are provided in Appendix F. In figure 5 the relaxation of a perturbed sphere is explored in a minimal setting. Already within this setting differences between the symmetric and asymmetric models with constant ($\beta = (2/3)$) and variable β can be observed. However, the full potential of the proposed models requires detailed parameter studies and should be investigated in comparison with molecular dynamics and experimental studies. One direction to be explored is the coexistence of a liquid-ordered and a liquid-disordered state. This can be achieved by modifying the idealised

https://doi.org/10.1017/jfm.2026.11474 Published online by Cambridge University Press

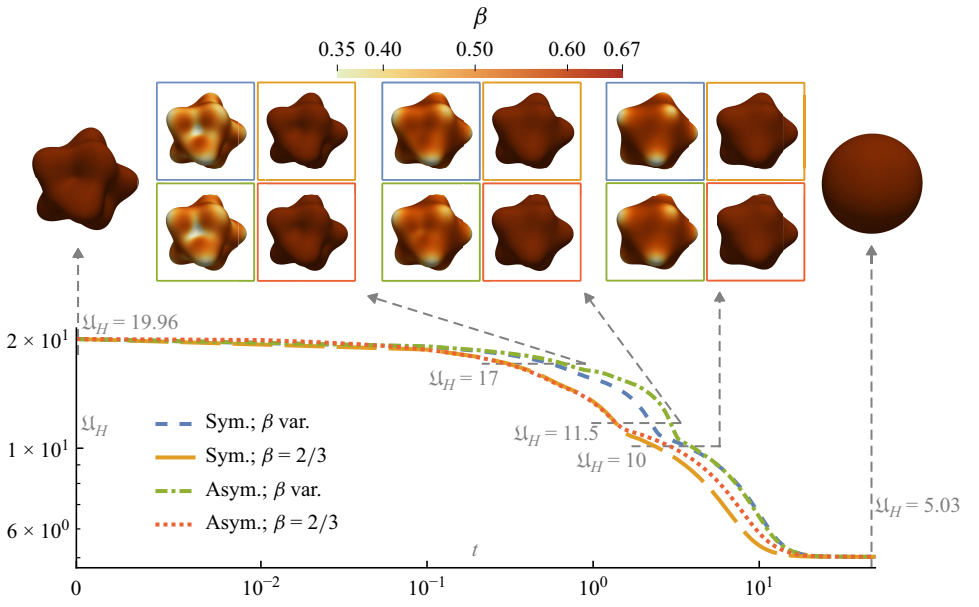


Figure 5. Evolution of the surface Beris–Edwards model (blue), the Navier–Stokes–Helfrich model with $\mathcal{H}_0 = 0$ (apricot), the hydrodynamic surface LH model (green) and the Navier–Stokes–Helfrich model with $\mathcal{H}_0 = -1.77$ (red). The parameters used are stated in Apppendix F. Shown is a double logarithmic plot of the time evolution of the Helfrich energy $\mathfrak{U}_H = \int_{\mathcal{S}} (\kappa/2)\mathcal{H}^2 \, d\mathcal{S}$, with $\kappa/2 = L = 0.1$, together with snapshots for different levels of $\mathfrak{U}_H$. Here $\mathfrak{U}_H = 19.96$ corresponds to the initial condition and $\mathfrak{U}_H = 5.03$ to the equilibrium configuration. In addition, we show intermediate states for $\mathfrak{U}_H = 17$, 11.5 and 10 for each model. The frames of the images follow the same colour coding as the plots. On the surface we show the value of the orientation field β in colour, ranging from $\beta = 0.35$ in light yellow to $\beta = 0.67$ in dark orange. While the shape corresponds to the same Helfrich energy and, therefore, only slightly differ, their appearance in time differs between the models with a slower shape evolution for variable β far away from the equilibrium state.

parameters in the thermotropic energy $\mathfrak{U}_{TH}$. This will link the hydrodynamic surface LH model for asymmetric lipid bilayers to models for two-phase systems of the Jülicher–Lipowski type (Jülicher & Lipowsky 1996; Baumgart *et al.* 2003; Lowengrub, Rätz & Voigt 2009; Elliott & Stinner 2010; Barrett, Garcke & Nürnberg 2017; Bachini *et al.* 2023*a*,*b*; Sischka & Voigt 2025). Phase coexistence between liquid-ordered and liquid-disordered phases still fall within the class of lipid bilayers, where the average lipid chain axis is approximately aligned with the membrane normal and orientational fluctuations are primarily captured by a scalar order parameter (Seifert 1997; Marsh 2013). This significantly simplifies the Q-tensor ansatz as the only remaining orientational degree of freedom is the scalar order parameter β. Situations involving pronounced molecular tilt, hydrophobic mismatch, faceted gel-phase vesicles or strong protein-induced director reorientation fall outside the scope of this simplified formulation. Dealing with such situations requires the general surface Beris–Edwards model (Nitschke & Voigt 2025*b*) to be endowed with a polarisation as considered in § 4.3 or at least retaining the surface non-conforming vector $\boldsymbol{\eta} \in T\mathcal{S}$ in (4.2) as a degree of freedom and describing the flat degenerate component $\boldsymbol{q} \in \mathcal{Q}^2\mathcal{S}$ as a function of $\boldsymbol{\eta}$ and β. Solving the uniaxaility condition $(\mathrm{Tr}\,\boldsymbol{Q}^2)^3 - 6(\mathrm{Tr}\,\boldsymbol{Q}^3)^2 = 0$ or $\boldsymbol{Q}^4 - (5/6)(\mathrm{Tr}\,\boldsymbol{Q}^2)\,\boldsymbol{Q}^2 + (1/9)(\mathrm{Tr}\,\boldsymbol{Q}^2)^2 \boldsymbol{Id} = \boldsymbol{0}$ (Nitschke & Voigt 2025*b*) leads to

$$\boldsymbol{q}(\boldsymbol{\eta}, \beta) = \frac{1}{2}\left(\sqrt{9\beta^2 + 8\|\boldsymbol{\eta}\|^2} - 3\beta\right)\left(\frac{\boldsymbol{\eta} \otimes \boldsymbol{\eta}}{\|\boldsymbol{\eta}\|^2} - \frac{1}{2}\boldsymbol{Id}_{\mathcal{S}}\right), \tag{5.1}$$

https://doi.org/10.1017/jfm.2026.11474 Published online by Cambridge University Press

where $\boldsymbol{q}(\boldsymbol{\eta}, \beta) \to \mathbf{0}$ holds for $\boldsymbol{\eta} \to \mathbf{0}$, which is the special case (4.1). Such an extension would already significantly increase both the modelling complexity and the effort required for a numerical approximation. We therefore refrain from pursuing this approach in the present paper. The same holds true for further model refinements, e.g. considering different leaflets or flip-flop mechanisms.

Funding. A.V. was supported by German Research Foundation (DFG) through FOR3013 'Vector- and tensor-valued surface PDEs'.

Declaration of interests. There are no competing interests.

Authors' contributions. This project was conceived by I.N., J.M.S. and A.V.; I.N. derived the theory, the results were analysed by I.N. and A.V., J.M.S. performed the simulations and the main text was written by I.N. and A.V.

Appendix A. Material parameter regime

The derivative part of the polarised surface Landau–de Gennes energy (4.22) is bounded below simply by $l_1 = 3L/2 \geq 0$. In contrast, the treatment of material parameters in the non-derivative part is not quite as straightforward. For this purpose, we define

$$\int_{\mathcal{S}} f \,\mathrm{d}\mathcal{S} := \mathfrak{U}_{LdG} - \frac{l_1}{2} \|\nabla\beta\|^2_{\mathrm{L}^2(T\mathcal{S})} \,. \tag{A1}$$

Since the surface area is finite, we consider only the energy density f in the following. Due to dependencies between mean curvature $\mathcal{H}$ and Gaussian curvature $\mathcal{K}$, we use the mutual independent principal curvatures κ_1 and κ_2 instead, i.e. we substitute $\mathcal{H} = \kappa_1 + \kappa_2$ and $\mathcal{K} = \kappa_1\kappa_2$. Therefore, f is a polynomial of fourth order in κ_1, κ_2 and β:

$$\begin{aligned}
f &= f_4 + f_3 + f_2, \\
f_4(\kappa_1, \kappa_2, \beta) &= \frac{l_0}{2}\left(\kappa_1^2 + \kappa_2^2\right)\beta^2 + \left(l_0 - \bar{l}_0\right)\kappa_1\kappa_2\beta^2 + \frac{k_3}{3}\left(\kappa_1 + \kappa_2\right)\beta^3 + \frac{C}{4}\beta^4, \\
f_3(\kappa_1, \kappa_2, \beta) &= \frac{k_2}{2}\left(\kappa_1 + \kappa_2\right)\beta^2 + \frac{B}{3}\beta^3, \\
f_2(\kappa_1, \kappa_2, \beta) &= k_1\left(\kappa_1 + \kappa_2\right)\beta + \frac{A}{2}\beta^2.
\end{aligned} \tag{A2}$$

The asymptotic behaviour is given by the leading polynomial f_4. Since, *a priori*, we see no reasons to restrict the material parameter $0 \leq \bar{l}_0 \leq l_0$ and $0 < C$ any further, we like to constrain the third-order polarising parameter k_3 in the following. The leading polynomial is evaluated in a spherical space in order to examine the asymptotic behaviour:

$$\begin{aligned}
&f_4(\kappa_1, \kappa_2, \beta) = f_4(r\cos\theta\sin\varphi, r\sin\theta\sin\varphi, r\cos\varphi) = r^4\frac{\cos^2\varphi}{12}s(\varphi, \theta), \\
&s(\varphi, \theta) = 6(l_0 + 2(l_0 - \bar{l}_0)\sin\theta\cos\theta)\sin^2\varphi + 4k_3(\cos\theta + \sin\theta)\sin\varphi\cos\varphi + 3C\cos^2\varphi \\
&= 6(l_0 + (l_0 - \bar{l}_0)\sin 2\theta)\sin^2\varphi + 2\sqrt{2}k_3\sin\left(\theta + \frac{\pi}{4}\right)\sin 2\varphi + 3C\cos^2\varphi.
\end{aligned} \tag{A3}$$

Here $\varphi \in [0, \pi]$ and $\theta \in [0, 2\pi)$, i.e. our argumentation is

$$\forall\varphi, \theta: \quad s(\varphi, \theta) > 0 \;\; \text{(to be shown)} \quad \Rightarrow \quad \lim_{r\to\infty} f_4 \in \{0, +\infty\} \quad \Rightarrow \quad f \text{ is bounded below.} \tag{A4}$$

Note that $\lim_{r\to\infty} f_4 = 0$ for $s > 0$ only happens if $\cos\varphi = 0$ is valid, i.e. $\beta = 0$ and hence $f = 0$.

https://doi.org/10.1017/jfm.2026.11474 Published online by Cambridge University Press

The function s has a unique minimum in φ, which can be computed by standard methods. (For instance, find $\varphi^* \in [0, \pi]$ such that $\partial_\varphi s(\varphi^*, \theta) = 0$ and $\partial_\varphi^2 s(\varphi^*, \theta) > 0$ is valid.) Therefore, we can bound s from below by

$$s(\varphi, \theta) \geq \min_{\varphi} s(\varphi, \theta) = \frac{1}{2}\left(a_s(\theta) + b_s - \sqrt{(a_s(\theta) - b_s)^2 + c_s(\theta)^2}\right), \tag{A5}$$

where

$$a_s(\theta) = 6\left(l_0 + \left(l_0 - \bar{l}_0\right)\sin 2\theta\right), \quad b_s = 3C, \quad c_s(\theta) = 4\sqrt{2}k_3 \sin\left(\theta + \frac{\pi}{4}\right). \tag{A6}$$

Since $a_s(\theta) \geq 0$ and $C > 0$, we can square $a_s(\theta) + b_s$ for the inequality $s(\varphi, \theta) > 0$ and obtain the simpler problem $4a_s(\theta)b_s - c_s(\theta)^2 > 0$. With $\sin^2(\theta + (\pi/4)) = (1/2)(1 + \sin 2\theta)$, this reads

$$\left(9C\left(l_0 - \bar{l}_0\right) - 2k_3^2\right)\sin 2\theta + 9Cl_0 - 2k_3^2 > 0, \tag{A7}$$

which must hold. For $k_3^2 \leq (9/2)C(l_0 - \bar{l}_0)$, this inequality is always valid, since the minimum in θ on the left-hand side yields $9C\bar{l}_0$, which is positive by $C > 0$ and $\bar{l}_0 \geq 0$. For $k_3^2 > (9/2)C(l_0 - \bar{l}_0)$, the minimum on the left-hand side yields $9C(2l_0 - \bar{l}_0) - 4k_3^2$. This results in the upper bound $k_3^2 < (9/4)C(2l_0 - \bar{l}_0)$, which is already less restrictive then the former $k_3^2 \leq (9/2)C(l_0 - \bar{l}_0)$. Ultimately, we conclude that

$$k_3 \in \left(-\frac{3}{2}\sqrt{C\left(2l_0 - \bar{l}_0\right)}, \frac{3}{2}\sqrt{C\left(2l_0 - \bar{l}_0\right)}\right) \tag{A8}$$

is sufficient for f to be bounded below. Note that the parameter interval (A8) is even sharp for f to be bounded below, up to the edge cases $k_3 = \pm(3/2)\sqrt{C(2l_0 - \bar{l}_0)}$, which would imply that we would also need to examine the lower-order polynomial f_3 and possibly even f_2. We shall not pursue these considerations here.

In the following, we align (A8) with the material parameters appearing in the surface LH energy (4.25). The parameter relations (4.26) yield

$$0 < \frac{9}{2}C\left(l_0 - \bar{l}_0\right) - k_3^2 = \frac{81}{128}\left(\left(8\hat{a} + 486\varpi\right)(2\kappa - \bar{\kappa}) - 81\kappa\bar{\kappa}\left(\mathcal{H}_0 - \hat{\mathcal{H}}_0\right)^2\right). \tag{A9}$$

Since the leading term is strictly positive, this inequality is satisfied for all special cases in which the second term vanishes, e.g. neglecting the Gaussian curvature ($\bar{\kappa} = 0$) or β-independent spontaneous curvature ($\mathcal{H}_0 = \hat{\mathcal{H}}_0$). In the general case, it is most natural to further restrict the double-well parameters $\hat{a}$, $\varpi > 0$ rather than the curvature parameters $\kappa \geqslant \bar{\kappa} \geqslant 0$ and $\mathcal{H}_0$, $\hat{\mathcal{H}}_0 \in \mathbb{R}$. This leads to

$$6\varpi + \frac{8}{81}\hat{a} > \frac{\kappa\bar{\kappa}}{2\kappa - \bar{\kappa}}\left(\mathcal{H}_0 - \hat{\mathcal{H}}_0\right)^2 > 0. \tag{A10}$$

It should be noted that this is not a substantive restriction, as both double-well parameters can be rescaled simultaneously, which only changes the double-well potential (4.24) by an overall prefactor, i.e. it is $f_{\gamma\varpi,\gamma\hat{a}} = \gamma f_{\varpi,\hat{a}}$ valid for all rescaling factors $\gamma > 1$.

https://doi.org/10.1017/jfm.2026.11474 Published online by Cambridge University Press

Appendix B. Variations

B.1. *Introduction*

Molecular force fields $\omega_\bullet \in T^0\mathcal{S}$, fluid force fields $\boldsymbol{F}_\bullet \in T\mathbb{R}^3|_\mathcal{S}$ and fluid stress fields $\boldsymbol{\Sigma}_\bullet \in T\mathbb{R}^3|_\mathcal{S} \otimes T\mathcal{S} < T^2\mathbb{R}^3|_\mathcal{S}$ are mostly defined in a usual way by

$$\begin{aligned}
\langle \omega_\bullet, \psi\rangle_{\mathrm{L}^2(T^0\mathcal{S})} &:= -\frac{2}{3}\left\langle \frac{\delta \mathfrak{U}_\bullet}{\delta \beta}, \psi\right\rangle_{\mathrm{L}^2(T^0\mathcal{S})}, & \langle \boldsymbol{F}_\bullet, \boldsymbol{W}\rangle_{\mathrm{L}^2(T\mathbb{R}^3|_\mathcal{S})} &:= -\left\langle \frac{\delta \mathfrak{U}_\bullet}{\delta \boldsymbol{X}}, \boldsymbol{W}\right\rangle_{\mathrm{L}^2(T\mathbb{R}^3|_\mathcal{S})},\\
\langle \omega_\bullet, \psi\rangle_{\mathrm{L}^2(T^0\mathcal{S})} &:= -\frac{2}{3}\left\langle \frac{\delta \mathfrak{R}_\bullet}{\delta \dot\beta}, \psi\right\rangle_{\mathrm{L}^2(T^0\mathcal{S})}, & \langle \boldsymbol{F}_\bullet, \boldsymbol{W}\rangle_{\mathrm{L}^2(T\mathbb{R}^3|_\mathcal{S})} &:= -\left\langle \frac{\delta \mathfrak{R}_\bullet}{\delta \boldsymbol{V}}, \boldsymbol{W}\right\rangle_{\mathrm{L}^2(T\mathbb{R}^3|_\mathcal{S})},\\
& & \langle \boldsymbol{\Sigma}_\bullet, \nabla_\mathsf{C}\boldsymbol{W}\rangle_{\mathrm{L}^2(T^2\mathbb{R}^3|_\mathcal{S})} &:= \langle \boldsymbol{F}_\bullet, \boldsymbol{W}\rangle_{\mathrm{L}^2(T\mathbb{R}^3|_\mathcal{S})}, \quad \text{(B1)}
\end{aligned}$$

for all virtual displacements $\psi \in T^0\mathcal{S}$ and $\boldsymbol{W} \in T\mathbb{R}^3|_\mathcal{S}$, see Nitschke & Voigt (2025*b*), i.e. it holds that

$$\boldsymbol{F}_\bullet = \boldsymbol{f}_\bullet + f_\bullet^\perp \boldsymbol{\nu} = \mathrm{Div}_\mathsf{C}\boldsymbol{\Sigma}_\bullet = \mathrm{Div}_\mathsf{C}\big(\boldsymbol{\sigma}_\bullet + \boldsymbol{\nu}\otimes\boldsymbol{\eta}_\bullet\big) = \mathrm{div}\boldsymbol{\sigma}_\bullet - \boldsymbol{II}\,\boldsymbol{\eta}_\bullet + \big(\mathrm{div}\boldsymbol{\eta}_\bullet + \boldsymbol{II} : \boldsymbol{\sigma}_\bullet\big)\boldsymbol{\nu}, \quad \text{(B2)}$$

where $\boldsymbol{\sigma}_\bullet \in T^2\mathcal{S}$ are the tangential stress fields, $\boldsymbol{\eta}_\bullet \in T\mathcal{S}$ the (tangential-)normal stress fields, $\boldsymbol{f}_\bullet \in T\mathcal{S}$ the tangential force fields, $f_\bullet^\perp \in T^0\mathcal{S}$ the normal force fields and $\bullet$ is a wildcard for the respective name indices, implicitly given by either a potential energy $\mathfrak{U}_\bullet$ or a flux potential $\mathfrak{R}_\bullet$. The factor $(2/3)$ in the definition of scalar order forces $\omega_\bullet$ is chosen for consistency with Nitschke & Voigt (2025*a*,*b*) and does not affect the scalar order equation $0 = \sum_\bullet \omega_\bullet$. Essentially, we merely evaluate this equation covariantly rather than contravariantly with respect to the lipid basis $(\boldsymbol{\nu}\otimes\boldsymbol{\nu} - (1/2)\boldsymbol{Id}_\mathcal{S})$ used in (4.1). The fluid equations are, according to the Lagrange–D'Alembert principle (Nitschke & Voigt 2025*b*), given by $\rho\boldsymbol{A} = \sum_\bullet \boldsymbol{F}_\bullet$, respectively $\rho\boldsymbol{a} = \sum_\bullet \boldsymbol{f}_\bullet$ in the tangential direction and $\rho a_\perp = \sum_\bullet f_\bullet^\perp$ in the normal direction, where $\boldsymbol{A} = \boldsymbol{a} + a_\perp\boldsymbol{\nu} = \mathrm{D}_t^\mathfrak{m}\boldsymbol{V}$ is the material acceleration; see (3.3) or table 5. Mass conservation is reduced to inextensibility ($\mathrm{Div}_\mathsf{C}\boldsymbol{V} = 0$) in the usual manner (Arroyo & DeSimone 2009; Nitschke & Voigt 2025*b*) by introducing a Lagrange multiplier, which plays the role of a pressure. For the sake of simplicity, we neglect all gauges of surface independence (Nitschke *et al.* 2023) (without loss of generality), i.e. $\eth_{\boldsymbol{W}}\beta = 0$ for all surface deformation directions $\boldsymbol{W} \in T\mathbb{R}^3|_\mathcal{S}$. The governing equations derived from the Lagrange-D'Alembert principle are invariant under any consistent choice of *a priori* independences between order parameter β and surface $\mathcal{S}$; cf. Nitschke & Voigt (2025*b*).

B.2. *Surface LH energy*

In this section we variate the surface LH energy (4.25)

$$\begin{aligned}
&\mathfrak{U}_{LH} = \int_\mathcal{S} u_1 + \frac{u_\kappa}{2}(\mathcal{H} - u_0)^2 - u_{\bar\kappa}\mathcal{K} + u_{\mathrm{d}w}\mathrm{d}\mathcal{S},\\
&\text{with}\quad u_0 = f_{\mathcal{H}_0,\hat{\mathcal{H}}_0}(\beta) = \hat{\mathcal{H}}_0 + \frac{3}{2}\big(\mathcal{H}_0 - \hat{\mathcal{H}}_0\big)\beta, \qquad u_1 = \frac{3}{4}L\,\|\nabla\beta\|_{T\mathcal{S}}^2,\\
&u_\kappa = f_\kappa(\beta) = \frac{9}{4}\kappa\beta^2, \qquad u_{\bar\kappa} = f_{\bar\kappa}(\beta) = \frac{9}{4}\bar\kappa\beta^2,\\
&u_{\mathrm{d}w} = f_{\varpi,\hat a}(\beta) = \frac{9}{4}\beta^2\left(\frac{\hat a}{9}\left(\frac{2}{3} - \beta\right)^2 - \frac{3\varpi}{2}\beta\left(4 - \frac{9}{2}\beta\right)\right). \quad \text{(B3)}
\end{aligned}$$

https://doi.org/10.1017/jfm.2026.11474 Published online by Cambridge University Press

Identifier	Expression	Naming
$\boldsymbol{a}$	$(\partial_t v^i)\partial_i \boldsymbol{X}_o + \boldsymbol{\nabla}_{\boldsymbol{v}-\boldsymbol{v}_o}\boldsymbol{v} + \boldsymbol{\nabla}_{\boldsymbol{v}}\boldsymbol{v}_o - v_\perp(\boldsymbol{\nabla} v_\perp + 2\boldsymbol{II}\,\boldsymbol{v})$	Tan. acceleration
$a_\perp$	$\partial_t v_\perp + \boldsymbol{\nabla}_{2\boldsymbol{v}-\boldsymbol{v}_o} v_\perp + \boldsymbol{II}(\boldsymbol{v},\boldsymbol{v})$	Nor. acceleration
$\mathrm{d}_t^{\mathcal{J}}\,\boldsymbol{q}$	$\mathfrak{J}\boldsymbol{q} = \dot{\boldsymbol{q}} - \boldsymbol{A}[\boldsymbol{V}]\boldsymbol{q} + \boldsymbol{q}\boldsymbol{A}[\boldsymbol{V}]$	Jaumann time derivative
$\mathrm{d}_t^{\mathfrak{m}}$	$\dot{\boldsymbol{q}} = (\partial_t q^{ij})\partial_i \boldsymbol{X}_o \otimes \partial_j \boldsymbol{X}_o + \boldsymbol{\nabla}_{\boldsymbol{v}-\boldsymbol{v}_o}\boldsymbol{q} + \boldsymbol{G}[\boldsymbol{V}_o]\boldsymbol{q} + \boldsymbol{q}\boldsymbol{G}^T[\boldsymbol{V}_o]$	Material time derivative
$\boldsymbol{\sigma}_{EL}$	$-L((\boldsymbol{\nabla}\boldsymbol{q})^T : \boldsymbol{\nabla}\boldsymbol{q} + \frac{3}{2}\boldsymbol{\nabla}\beta \otimes \boldsymbol{\nabla}\beta - \frac{1}{4}(2\|\boldsymbol{\nabla}\boldsymbol{q}\|^2_{T^3\mathcal{S}} + 3\|\boldsymbol{\nabla}\beta\|^2_{T^2\mathcal{S}})\boldsymbol{Id}_{\mathcal{S}} - 6\mathcal{K}\beta\boldsymbol{q} + \frac{1}{2}(2\mathcal{H}\mathrm{Tr}\boldsymbol{q}^2 - 12\beta\boldsymbol{q} : \boldsymbol{II} + 9\mathcal{H}\beta^2)(\boldsymbol{II} - \frac{\mathcal{H}}{2}\boldsymbol{Id}_{\mathcal{S}}))$	Elastic stress
$\boldsymbol{\zeta}_{EL}$	$L(2(\boldsymbol{\nabla}\boldsymbol{q}) : \boldsymbol{II} + \boldsymbol{q}\boldsymbol{\nabla}\mathcal{H} - 3\boldsymbol{II}\boldsymbol{\nabla}\beta - \frac{3}{2}\beta\boldsymbol{\nabla}\mathcal{H})$	Elastic pt. of surface-conforming constr.
$\boldsymbol{h}_{EL}$	$L(\Delta\boldsymbol{q} - (\mathcal{H}^2 - 2\mathcal{K})\boldsymbol{q} + 3\beta\mathcal{H}(\boldsymbol{II} - \frac{\mathcal{H}}{2}\boldsymbol{Id}_{\mathcal{S}}))$	Tan. mol. elastic force
ω_{EL}	$L(\Delta\beta + 2\mathcal{H}\boldsymbol{II} : \boldsymbol{q} - 3\beta(\mathcal{H}^2 - 2\mathcal{K}))$	Nor. mol. elastic force
$\boldsymbol{h}_{TH}$	$-(2a - 2b\beta + 3c\beta^2 + 2c\mathrm{Tr}\boldsymbol{q}^2)\boldsymbol{q}$	Tan. mol. thermotropic force
ω_{TH}	$-(2a + b\beta + 3c\beta^2 + 2c\mathrm{Tr}\boldsymbol{q}^2)\beta + \frac{2}{3}b\mathrm{Tr}\boldsymbol{q}^2$	Nor. mol. thermotropic force
$f_{BE}^{\perp}$	$-\kappa(\Delta\mathcal{H} + (\mathcal{H} - \mathcal{H}_0)(\frac{1}{2}\mathcal{H}(\mathcal{H} + \mathcal{H}_0) - 2\mathcal{K}))$	Bending force
$\boldsymbol{\sigma}_{IM}^{\mathcal{J}}$	$M(\boldsymbol{q}\mathfrak{J}\boldsymbol{q} - (\mathfrak{J}\boldsymbol{q})\boldsymbol{q})$	Jaumann immobility stress
$\boldsymbol{\sigma}_{IM}^{\mathfrak{m}}$	$\boldsymbol{0}$	Material immobility stress
$\boldsymbol{\zeta}_{IM}^{\mathcal{J}}$	$\boldsymbol{0}$	Jaumann immobility pt. of surface-conforming constr.
$\boldsymbol{\zeta}_{IM}^{\mathfrak{m}}$	$-M(\boldsymbol{\nabla} v_\perp + \boldsymbol{v}\boldsymbol{II})(\boldsymbol{q} - \frac{3}{2}\beta\boldsymbol{Id}_{\mathcal{S}})$	Material immobility pt. of surface-conforming constr.
$\boldsymbol{\sigma}_{NV}^0$	$2\upsilon\boldsymbol{S}[\boldsymbol{V}]$	Iso. viscosity stress
$\boldsymbol{\sigma}_{NV}^1$ ($\mathcal{J}$-form)	$-\upsilon(\mathfrak{J}\boldsymbol{q} - \frac{\dot{\beta}}{2}\boldsymbol{Id}_{\mathcal{S}} + 3\boldsymbol{q}\boldsymbol{S}[\boldsymbol{V}] + \boldsymbol{S}[\boldsymbol{V}]\boldsymbol{q} - 2\beta\boldsymbol{S}[\boldsymbol{V}])$	1st ord. aniso. viscosity stress
$\boldsymbol{\sigma}_{NV}^1$ ($\mathfrak{m}$-form)	$-\upsilon(\dot{\boldsymbol{q}} - \frac{\dot{\beta}}{2}\boldsymbol{Id}_{\mathcal{S}} + \boldsymbol{q}(2\boldsymbol{G}[\boldsymbol{V}] + \boldsymbol{G}^T[\boldsymbol{V}]) + \boldsymbol{G}^T[\boldsymbol{V}]\boldsymbol{q} - 2\beta\boldsymbol{S}[\boldsymbol{V}])$	1st ord. aniso. viscosity stress

Table 5. For caption see next page.

https://doi.org/10.1017/jfm.2026.11474 Published online by Cambridge University Press

Identifier	Expression	Naming
$\boldsymbol{h}^1_{NV}$	$\upsilon \boldsymbol{S}[\boldsymbol{V}]$	1st ord. mol. aniso. viscosity force
$\boldsymbol{\sigma}^2_{NV}$ ($\mathcal{J}$-form)	$\upsilon(\boldsymbol{q}\mathfrak{J}\boldsymbol{q} - \frac{1}{2}(\beta\mathfrak{J}\boldsymbol{q} + \dot{\beta}\boldsymbol{q}) + \frac{1}{4}\beta\dot{\beta}\boldsymbol{Id}_{\mathcal{S}} + \boldsymbol{q}\boldsymbol{S}[\boldsymbol{V}]\boldsymbol{q} - \frac{1}{2}\beta(3\boldsymbol{q}\boldsymbol{S}[\boldsymbol{V}] + \boldsymbol{S}[\boldsymbol{V}]\boldsymbol{q}) + \frac{1}{2}(\mathrm{Tr}\boldsymbol{q}^2 + \beta^2)\boldsymbol{S}[\boldsymbol{V}])$	2nd ord. aniso. viscosity stress
$\boldsymbol{\sigma}^2_{NV}$ (m-form)	$\upsilon(\boldsymbol{q}\dot{\boldsymbol{q}} - \frac{1}{2}(\beta\dot{\boldsymbol{q}} + \dot{\beta}\boldsymbol{q}) + \frac{1}{4}\beta\dot{\beta}\boldsymbol{Id}_{\mathcal{S}} + \boldsymbol{q}\boldsymbol{G}^T[\boldsymbol{V}]\boldsymbol{q} - \frac{1}{2}\beta(\boldsymbol{q}(2\boldsymbol{G}[\boldsymbol{V}] + \boldsymbol{G}^T[\boldsymbol{V}]) + \boldsymbol{G}^T[\boldsymbol{V}]\boldsymbol{q}) + \frac{1}{2}(\mathrm{Tr}\boldsymbol{q}^2)\boldsymbol{G}[\boldsymbol{V}] + \frac{1}{2}\beta^2\boldsymbol{S}[\boldsymbol{V}])$	2nd ord. aniso. viscosity stress
$\widetilde{\boldsymbol{h}}^{2,\mathcal{J}}_{NV}$	$-\frac{\upsilon}{2}(\boldsymbol{q}\boldsymbol{S}[\boldsymbol{V}] + \boldsymbol{S}[\boldsymbol{V}]\boldsymbol{q} - (\boldsymbol{q} : \boldsymbol{G}[\boldsymbol{V}])\boldsymbol{Id}_{\mathcal{S}} - \beta\boldsymbol{S}[\boldsymbol{V}])$	Pt. of 2nd ord. mol. aniso. viscosity force
$\widetilde{\boldsymbol{h}}^{2,\mathfrak{m}}_{NV}$	$-\frac{\upsilon}{2}(\boldsymbol{q}\boldsymbol{G}[\boldsymbol{V}] + \boldsymbol{G}^T[\boldsymbol{V}]\boldsymbol{q} - (\boldsymbol{q} : \boldsymbol{G}[\boldsymbol{V}])\boldsymbol{Id}_{\mathcal{S}} - \beta\boldsymbol{S}[\boldsymbol{V}])$	Pt. of 2nd ord. mol. aniso. viscosity force
$\widetilde{\omega}^2_{NV}$	$\frac{\upsilon}{3}\boldsymbol{q} : \boldsymbol{G}[\boldsymbol{V}]$	Pt. of 2nd ord. mol. aniso. viscosity force
$\boldsymbol{\sigma}_{NA}$	$\alpha_{\mathrm{NA}}\boldsymbol{q}$	Nematic activity stress

Table 5. (cntd). Necessary terms for the surface-conforming Beris–Edwards models (D1) for a consistent choice $\Phi \in \{\mathcal{J}, \mathfrak{m}\}$. These representations comprise the tangential deformation gradient $\boldsymbol{G}[\boldsymbol{V}] = \nabla\boldsymbol{v} - v_\perp\boldsymbol{II}$ of the material velocity $\boldsymbol{V} = \boldsymbol{v} + v_\perp\boldsymbol{\nu}$. Here $\boldsymbol{S}[\boldsymbol{V}]$ and $\boldsymbol{A}[\boldsymbol{V}]$ are its symmetric and skew-symmetric part. Time derivatives are determined with respect to an observer velocity $\boldsymbol{V}_o = \boldsymbol{v}_o + v_\perp\boldsymbol{\nu}$. For more details, see Nitschke & Voigt (2025*a*,*b*).

Except for the $u_{\bar{\kappa}}$ term, we can fully make use of Bachini *et al.* (2023*a*). The difference is merely semantic: instead of a density function, we have a scalar order parameter.

For $\mathfrak{U}_1 := \int_{\mathcal{S}} u_1 \mathrm{d}\mathcal{S}$, Bachini *et al.* (2023*a*) showed that we obtain

$$\begin{aligned} &\omega_1 = L\Delta\beta\,, \qquad \boldsymbol{\sigma}_1 = -\frac{3}{2}L\left(\nabla\beta\otimes\nabla\beta - \frac{\|\nabla\beta\|^2_{T\mathcal{S}}}{2}\boldsymbol{Id}_{\mathcal{S}}\right), \quad \boldsymbol{\eta}_1 = \boldsymbol{0}, \\ &\boldsymbol{f}_1 = -\frac{3}{2}\omega_1\nabla\beta, \quad f_1^\perp = -\frac{3}{2}L\left(\nabla\beta\,\boldsymbol{II}\,\nabla\beta - \frac{\mathcal{H}}{2}\|\nabla\beta\|^2\right). \end{aligned} \tag{B4}$$

For $\mathfrak{U}_0 := \int_{\mathcal{S}} (u_\kappa/2)(\mathcal{H} - u_0)^2 \mathrm{d}\mathcal{S}$, Bachini *et al.* (2023*a*) showed that we obtain

$$\begin{aligned} &\frac{3}{2}\omega_0 = -\frac{\partial_\beta u_\kappa}{2}(\mathcal{H}-u_0)^2 + u_\kappa(\partial_\beta u_0)(\mathcal{H}-u_0), && \boldsymbol{\sigma}_0 = -u_\kappa(\mathcal{H}-u_0)\Big(\boldsymbol{II} - \frac{\mathcal{H}-u_0}{2}\boldsymbol{Id}_{\mathcal{S}}\Big), \\ &\boldsymbol{f}_0 = -\frac{3}{2}\omega_0\nabla\beta, && \boldsymbol{\eta}_0 = -\nabla(u_\kappa(\mathcal{H}-u_0)), \\ &f_0^\perp = -\Delta(u_\kappa(\mathcal{H}-u_0)) - \frac{u_\kappa}{2}(\mathcal{H}-u_0)(\mathcal{H}(\mathcal{H}+u_0) - 4\mathcal{K}). \end{aligned} \tag{B5}$$

https://doi.org/10.1017/jfm.2026.11474 Published online by Cambridge University Press

Expanding the functions u_κ and u_0, and evaluating all derivatives, leads to

$$\begin{aligned}
\omega_0 &= -\frac{3}{2}\kappa\beta\left(\mathcal{H}-\hat{\mathcal{H}}_0-\frac{3}{2}(\mathcal{H}_0-\hat{\mathcal{H}}_0)\beta\right)\left(\mathcal{H}-\hat{\mathcal{H}}_0-3(\mathcal{H}_0-\hat{\mathcal{H}}_0)\beta\right),\\
\sigma_0 &= -\frac{9}{8}\kappa\beta^2\left(\mathcal{H}-\hat{\mathcal{H}}_0-\frac{3}{2}(\mathcal{H}_0-\hat{\mathcal{H}}_0)\beta\right)\left(2\boldsymbol{II}-\left(\mathcal{H}-\hat{\mathcal{H}}_0-\frac{3}{2}(\mathcal{H}_0-\hat{\mathcal{H}}_0)\beta\right)\boldsymbol{Id}_{\mathcal{S}}\right),\\
\boldsymbol{\eta}_0 &= -\frac{9}{4}\kappa\beta\left(\beta\nabla\mathcal{H}+2\left(\mathcal{H}-\hat{\mathcal{H}}_0-\frac{9}{4}(\mathcal{H}_0-\hat{\mathcal{H}}_0)\beta\right)\nabla\beta\right),\\
f_0^{\perp} &= -\frac{9}{4}\kappa\Bigg(\beta^2\Delta\mathcal{H}+2\beta\left(\mathcal{H}-\hat{\mathcal{H}}_0-\frac{9}{4}(\mathcal{H}_0-\hat{\mathcal{H}}_0)\beta\right)\Delta\beta\\
&\quad+2\left\langle 2\beta\nabla\mathcal{H}+\left(\mathcal{H}-\hat{\mathcal{H}}_0-\frac{9}{2}(\mathcal{H}_0-\hat{\mathcal{H}}_0)\beta\right)\nabla\beta,\nabla\beta\right\rangle_{T\mathcal{S}}\\
&\quad+\frac{\beta^2}{2}\left(\left(\mathcal{H}^2-\left(\hat{\mathcal{H}}_0+\frac{3}{2}(\mathcal{H}_0-\hat{\mathcal{H}}_0)\beta\right)^2\right)\mathcal{H}-4\left(\mathcal{H}-\hat{\mathcal{H}}_0-\frac{3}{2}(\mathcal{H}_0-\hat{\mathcal{H}}_0)\beta\right)\mathcal{K}\right)\Bigg).
\end{aligned}\tag{B6}$$

Unfortunately, the energy part $\mathfrak{U}_{\bar\kappa} := -\int_{\mathcal{S}} u_{\bar\kappa}\mathcal{K}\mathrm{d}\mathcal{S}$ is not treated in Bachini *et al.* (2023*a*) in any way. Therefore, we derive the variations of this energy in the following. The deformation derivative $\eth_{\boldsymbol{W}}\mathcal{K}$ of the Gaussian curvature $\mathcal{K}$ in deformation direction $\boldsymbol{W}\in T\mathbb{R}^3|_{\mathcal{S}}$ is given in Sischka *et al.* (2025):

$$\eth_{\boldsymbol{W}}\mathcal{K} = \langle\mathcal{H}\boldsymbol{Id}_{\mathcal{S}}-\boldsymbol{II},\nabla(\boldsymbol{v}\nabla_{\mathsf{C}}\boldsymbol{W})\rangle_{T^2\mathcal{S}}-\mathcal{K}\mathrm{Div}_{\mathsf{C}}\boldsymbol{W}.\tag{B7}$$

This and $\eth_{\boldsymbol{W}}\beta\equiv 0$, without loss of generality, leads to the spatial variation

$$\begin{aligned}
\left\langle\frac{\delta\mathfrak{U}_{\bar\kappa}}{\delta\boldsymbol{X}},\boldsymbol{W}\right\rangle_{\mathrm{L}^2(T\mathbb{R}^3|_{\mathcal{S}})} &= -\int_{\mathcal{S}} u_{\bar\kappa}\left(\eth_{\boldsymbol{W}}\mathcal{K}+\mathcal{K}\mathrm{Div}_{\mathsf{C}}\boldsymbol{W}\right)\mathrm{d}\mathcal{S}\\
&= -\left\langle u_{\bar\kappa}\left(\mathcal{H}\boldsymbol{Id}_{\mathcal{S}}-\boldsymbol{II}\right),\nabla(\boldsymbol{v}\nabla_{\mathsf{C}}\boldsymbol{W})\right\rangle_{\mathrm{L}^2(T^2|_{\mathcal{S}})}\\
&= \left\langle\boldsymbol{v}\otimes\mathrm{div}\left(u_{\bar\kappa}\left(\mathcal{H}\boldsymbol{Id}_{\mathcal{S}}-\boldsymbol{II}\right)\right),\nabla_{\mathsf{C}}\boldsymbol{W}\right\rangle_{\mathrm{L}^2(T^2\mathbb{R}^3|_{\mathcal{S}})},
\end{aligned}\tag{B8}$$

i.e. with $\mathrm{div}(\mathcal{H}\boldsymbol{Id}_{\mathcal{S}}-\boldsymbol{II})=\boldsymbol{0}$, we obtain

$$\boldsymbol{\sigma}_{\bar\kappa}=\boldsymbol{0},\qquad \boldsymbol{\eta}_{\bar\kappa}=\frac{9}{2}\bar\kappa\beta\left(\mathcal{H}\boldsymbol{Id}_{\mathcal{S}}-\boldsymbol{II}\right)\nabla\beta\tag{B9}$$

for the associated stress. Forces are given by

$$\begin{aligned}
\omega_{\bar\kappa} &= \frac{2}{3}(\partial_\beta u_{\bar\kappa})\mathcal{K}=3\bar\kappa\mathcal{K}\beta,\\
\boldsymbol{f}_{\bar\kappa} &= -\boldsymbol{II}\,\boldsymbol{\eta}_{\bar\kappa}=-\frac{9}{2}\bar\kappa\mathcal{K}\beta\nabla\beta=-\frac{3}{2}\omega_{\bar\kappa}\nabla\beta,\\
f_{\bar\kappa}^{\perp} &= \mathrm{div}\,\boldsymbol{\eta}_{\bar\kappa}=-\frac{9}{2}\bar\kappa\left(\beta\boldsymbol{II}:\nabla^2\beta-\mathcal{H}\beta\Delta\beta+(\nabla\beta)\boldsymbol{II}\nabla\beta-\mathcal{H}\|\nabla\beta\|^2_{T\mathcal{S}}\right),
\end{aligned}\tag{B10}$$

where we used the fact that $\boldsymbol{II}^2=\mathcal{H}\boldsymbol{II}-\mathcal{K}\boldsymbol{Id}_{\mathcal{S}}$ is valid.

https://doi.org/10.1017/jfm.2026.11474 Published online by Cambridge University Press

For the double-well potential $\mathfrak{U}_{\mathrm{dw}} := \int_{\mathcal{S}} u_{\mathrm{dw}} \mathrm{d}\mathcal{S}$, we can once more employ Bachini *et al.* (2023*a*) and obtain

$$\begin{aligned} u_{\mathrm{dw}} &= \frac{9}{4}\beta^2\left(\frac{\hat{a}}{9}\left(\frac{2}{3}-\beta\right)^2 - \frac{3\varpi}{2}\beta\left(4-\frac{9}{2}\beta\right)\right), & \boldsymbol{\sigma}_{\mathrm{dw}} &= u_{\mathrm{dw}}\boldsymbol{Id}_{\mathcal{S}}, \\ \omega_{\mathrm{dw}} &= -\frac{2}{3}\partial_\beta u_{\mathrm{dw}} = -\frac{1}{6}\beta\left(\frac{2}{3}-\beta\right)\left(4\hat{a}\left(\frac{1}{3}-\beta\right) - 243\varpi\beta\right), & \boldsymbol{\eta}_{\mathrm{dw}} &= \boldsymbol{0}, \\ \boldsymbol{f}_{\mathrm{dw}} &= \boldsymbol{\nabla} u_{\mathrm{dw}} = -\frac{3}{2}\omega_{\mathrm{dw}}\boldsymbol{\nabla}\beta, & f^{\perp}_{\mathrm{dw}} &= \mathcal{H}u_{\mathrm{dw}}. \end{aligned} \tag{B11}$$

It should be noted that the fluid force $\boldsymbol{F}_{\mathrm{dw}} = \boldsymbol{f}_{\mathrm{dw}} + f^{\perp}_{\mathrm{dw}}\boldsymbol{\nu}$ is not an applied force in inextensible materials and could be neglected, since $\boldsymbol{F}_{\mathrm{dw}} = \mathrm{Grad}_{\mathsf{C}} u_{\mathrm{dw}}$ is a pure pressure force.

B.3. *Flux potentials*

As demonstrated in § 4.2, the lipid ansatz (4.1) can be used without considering additional lipid constraint forces. Consequently, the flux forces and stresses of the surface-conforming model in Appendix D may also be evaluated with $\boldsymbol{q} = \boldsymbol{0}$. However, it is useful to explicitly write down the flux potentials resulting from the ansatz (4.1) for a better understanding, and to employ the corresponding variations as an additional means of verification, since 'Variation∘Restriction' is commutative in the absence of constraints forces. Nevertheless, we will keep the following calculations brief.

By the lipid ansatz (4.1) the anisotropic fluid metric yields

$$\boldsymbol{I}_\xi[\beta] := \boldsymbol{I}_\xi[\boldsymbol{Q}] = \boldsymbol{Id} - \xi\,\boldsymbol{Q} = \left(1+\frac{\xi}{2}\beta\right)\boldsymbol{Id}_{\mathcal{S}} + (1-\xi\beta)\,\boldsymbol{\nu}\otimes\boldsymbol{\nu}, \tag{B12}$$

where $\xi \in \mathbb{R}$ is the anisotropy coefficient. Its temporal distortion is given by the lower-convected rate (Nitschke & Voigt 2023)

$$\mathrm{D}_t^\flat\, \boldsymbol{I}_\xi[\beta] = \left(1+\frac{\xi}{2}\beta\right)\boldsymbol{Id}_{\mathcal{S}}\left(\boldsymbol{\nabla}_{\mathsf{C}}\boldsymbol{V} + \boldsymbol{\nabla}_{\mathsf{C}}^T\boldsymbol{V}\right)\boldsymbol{Id}_{\mathcal{S}} - \xi\dot{\beta}\left(\boldsymbol{\nu}\otimes\boldsymbol{\nu} - \frac{1}{2}\boldsymbol{Id}_{\mathcal{S}}\right) \tag{B13}$$

and determine the heat released by material deformations modulo rigid-body motions. The associated viscous flux potential $\mathfrak{R}_{NV} = (\upsilon/4)\| \mathrm{D}_t^\flat\, \boldsymbol{I}_\xi[\beta]\|^2_{\mathrm{L}^2(T^2\mathbb{R}^3|_{\mathcal{S}})}$ reads

$$\begin{aligned} \mathfrak{R}_{NV} = \frac{\upsilon}{8}\Bigg(2\left\|\left(1+\frac{\xi}{2}\beta\right)\boldsymbol{Id}_{\mathcal{S}}\left(\boldsymbol{\nabla}_{\mathsf{C}}\boldsymbol{V} + \boldsymbol{\nabla}_{\mathsf{C}}^T\boldsymbol{V}\right)\boldsymbol{Id}_{\mathcal{S}}\right\|^2_{\mathrm{L}^2(T^2\mathcal{S})} \\ + 3\xi^2\left\|\dot{\beta}\right\|^2_{\mathrm{L}^2(T^2\mathcal{S})} + 4\xi\left\langle\left(1+\frac{\xi}{2}\beta\right)\dot{\beta}, \mathrm{Div}_{\mathsf{C}}\boldsymbol{V}\right\rangle\Bigg)^2_{\mathrm{L}^2(T^2\mathcal{S})}, \end{aligned} \tag{B14}$$

where $\upsilon \geq 0$ is the isotropic viscosity. Variation with respect to process variables $\dot{\beta}$ and $\boldsymbol{V} = \boldsymbol{v} + v_\perp\boldsymbol{\nu}$ yields

https://doi.org/10.1017/jfm.2026.11474 Published online by Cambridge University Press

$$\omega_{\mathrm{NV}} = -\xi\upsilon\left(\frac{\xi}{2}\dot{\beta} + \frac{1}{3}\left(1+\frac{\xi}{2}\beta\right)(\mathrm{div}\boldsymbol{v} - \mathcal{H}v_\perp)\right),$$
$$\boldsymbol{\sigma}_{NV} = \upsilon\left(\left(1+\frac{\xi}{2}\beta\right)^2\left(\boldsymbol{\nabla v} + \boldsymbol{\nabla}^T\boldsymbol{v} - 2v_\perp\boldsymbol{II}\right) + \frac{\xi}{2}\dot{\beta}\left(1+\frac{\xi}{2}\beta\right)\boldsymbol{Id}_{\mathcal{S}}\right), \quad \boldsymbol{\eta}_{NV} = \boldsymbol{0}, \tag{B15}$$

which equals the viscosity contributions in the surface-conforming model in Appendix D, respectively Nitschke & Voigt (2025*b*), for $\boldsymbol{q} = \boldsymbol{0}$. It should be noted that, in inextensible materials, the trailing summands can be neglected since they either vanish or lead to a pressure gradient. Note that, for comparisons with table 5, it holds that $\omega_{NV} = \xi^2(\tilde{\omega}^2_{NV} - \upsilon\dot{\beta}/2)$ and $\boldsymbol{\sigma}_{NV} = \boldsymbol{\sigma}^0_{NV} + \xi\boldsymbol{\sigma}^1_{NV} + \xi^2\boldsymbol{\sigma}^2_{NV}$. Although we would not recommend proceeding in this way, for completeness, the tangential and normal fluid forces for isotropic viscous fluids ($\xi = 0$) are

$$\begin{aligned}\boldsymbol{f}_{iso} &:= \upsilon\mathrm{div}\left(\boldsymbol{\nabla v} + \boldsymbol{\nabla}^T\boldsymbol{v} - 2v_\perp\boldsymbol{II}\right)\\ &= \upsilon\left(\Delta\boldsymbol{v} + \mathcal{K}\boldsymbol{v} - 2\left(\boldsymbol{II} - \frac{\mathcal{H}}{2}\boldsymbol{Id}_{\mathcal{S}}\right)\boldsymbol{\nabla}v_\perp - v_\perp\boldsymbol{\nabla}\mathcal{H} + \boldsymbol{\nabla}(\mathrm{div}\boldsymbol{v} - v_\perp\mathcal{H})\right),\\ f^\perp_{iso} &:= \upsilon\boldsymbol{II} : \left(\boldsymbol{\nabla v} + \boldsymbol{\nabla}^T\boldsymbol{v} - 2v_\perp\boldsymbol{II}\right) = 2\upsilon\left(\boldsymbol{II} : \boldsymbol{\nabla v} - v_\perp\left(\mathcal{H}^2 - \mathcal{K}\right)\right),\end{aligned} \tag{B16}$$

see Arroyo & DeSimone (2009), Reuther *et al.* (2020), and yield the more general forces

$$\begin{aligned}\boldsymbol{f}_{NV} &= \left(1+\frac{\xi}{2}\beta\right)^2\boldsymbol{f}_{iso}\\ &\quad + \upsilon\left(\xi\left(1+\frac{\xi}{2}\beta\right)\left(\boldsymbol{\nabla v} + \boldsymbol{\nabla}^T\boldsymbol{v} - 2v_\perp\boldsymbol{II}\right)\boldsymbol{\nabla}\beta + \frac{\xi^2}{4}\dot{\beta}\boldsymbol{\nabla}\beta + \frac{\xi}{2}\left(1+\frac{\xi}{2}\beta\right)\boldsymbol{\nabla}\dot{\beta}\right),\\ f^\perp_{NV} &= \left(1+\frac{\xi}{2}\beta\right)^2 f^\perp_{iso} + \frac{\xi\upsilon}{2}\dot{\beta}\left(1+\frac{\xi}{2}\beta\right)\mathcal{H}.\end{aligned} \tag{B17}$$

Next, we address the immobility flux potential $\mathfrak{R}^\Phi_{IM} = \dfrac{M}{2}\left\|\mathrm{D}^\Phi_t\boldsymbol{Q}\right\|^2_{\mathrm{L}^2(T^2\mathbb{R}|_{\mathcal{S}})}$ with $\Phi \in \{\mathfrak{m}, \mathcal{J}\}$, where

$$\begin{aligned}\mathrm{D}^{\mathfrak{m}}_t\boldsymbol{Q} &= \dot{\beta}\left(\boldsymbol{v}\otimes\boldsymbol{v} - \frac{1}{2}\boldsymbol{Id}_{\mathcal{S}}\right) - \frac{3}{2}\beta\left(\boldsymbol{v}\boldsymbol{\nabla}_{\mathsf{C}}\boldsymbol{V}\otimes\boldsymbol{v} + \boldsymbol{v}\otimes\boldsymbol{v}\boldsymbol{\nabla}_{\mathsf{C}}\boldsymbol{V}\right),\\ \mathrm{D}^{\mathcal{J}}_t\boldsymbol{Q} &= \dot{\beta}\left(\boldsymbol{v}\otimes\boldsymbol{v} - \frac{1}{2}\boldsymbol{Id}_{\mathcal{S}}\right)\end{aligned} \tag{B18}$$

holds by Nitschke & Voigt (2023) and lipid ansatz (4.1). This results in

$$\mathfrak{R}^{\mathfrak{m}}_{IM} = \frac{3M}{4}\left(\left\|\dot{\beta}\right\|^2_{L^2(T^0\mathcal{S})} + 3\left\|\beta\upsilon\boldsymbol{\nabla}_{\mathsf{C}}\boldsymbol{V}\right\|^2_{\mathrm{L}^2(T\mathcal{S})}\right), \quad \mathfrak{R}^{\mathcal{J}}_{IM} = \frac{3M}{4}\left\|\dot{\beta}\right\|^2_{\mathrm{L}^2(T^0\mathcal{S})}. \tag{B19}$$

Variation with respect to process variables $\dot{\beta}$ and $\boldsymbol{V} = \boldsymbol{v} + v_\perp\boldsymbol{\nu}$ yields

$$\begin{aligned}&\omega^{\mathfrak{m}}_{IM} = \omega^{\mathcal{J}}_{IM} = -M\dot{\beta},\\ &\boldsymbol{\sigma}^{\mathfrak{m}}_{IM} = \boldsymbol{\sigma}^{\mathcal{J}}_{IM} = \boldsymbol{0}, \qquad \boldsymbol{\eta}^{\mathfrak{m}}_{IM} = \frac{9M}{2}\beta^2\left(\boldsymbol{\nabla}v_\perp + \boldsymbol{II}\,\boldsymbol{v}\right), \quad \boldsymbol{\eta}^{\mathcal{J}}_{IM} = \boldsymbol{0}.\end{aligned} \tag{B20}$$

https://doi.org/10.1017/jfm.2026.11474 Published online by Cambridge University Press

This also agrees with the surface-conforming model in Appendix D, respectively Nitschke & Voigt (2025*b*), for $\boldsymbol{q}=\boldsymbol{0}$. It should be noted that the surface-conforming model does not impose any normal immobility stresses $\boldsymbol{\eta}^{\Phi}_{IM}$ directly. Instead, it comprises constraint forces to ensure surface conformity, e.g. in terms of $\boldsymbol{\zeta}^{\Phi}_{IM}T\mathcal{S}$. However, the lipid ansatz (4.1) already stipulates surface conformity *a priori*. Both procedures are equivalent eventually and, for $\boldsymbol{q}=\boldsymbol{0}$, it holds that $\boldsymbol{\eta}^{\Phi}_{IM}=3\beta\boldsymbol{\zeta}^{\Phi}_{IM}$ and, thus, gives the same immobility force in the fluid equation. For the sake of completeness, the resulting fluid forces in tangential and normal directions are

$$\begin{aligned} \boldsymbol{f}^{\mathfrak{m}}_{IM} &= \frac{9M}{2}\beta^2\left(\mathcal{K}\boldsymbol{v}-\boldsymbol{II}\left(\nabla v_\perp+\mathcal{H}\boldsymbol{v}\right)\right), & \boldsymbol{f}^{\mathcal{J}}_{IM}&=\boldsymbol{0},\\ f^{\mathfrak{m},\perp}_{IM} &= \frac{9M}{2}\beta\left(\left(\Delta v_\perp+\boldsymbol{II}:\nabla\boldsymbol{v}+\nabla_{\boldsymbol{v}}\mathcal{H}\right)\beta+2\left(\nabla v_\perp+\boldsymbol{v}\boldsymbol{II}\right)\nabla\beta\right), & f^{\mathcal{J},\perp}_{IM}&=0. \end{aligned} \tag{B21}$$

The activity flux potential $\mathfrak{R}_{AC}=(\alpha/2)\int_{\mathcal{S}}(\mathrm{Tr}\circ\mathrm{D}_t^{\flat}\boldsymbol{I}_\xi[\boldsymbol{Q}])\mathrm{d}\mathcal{S}$, which stated the first moment of the temporal anisotropic metric distortion, is not relevant for lipids on an inextensible medium. This can be seen by (B13), which yields

$$\mathfrak{R}_{AC}=\alpha\int_{\mathcal{S}}\left(1+\frac{\xi}{2}\beta\right)\mathrm{Div}_{\mathsf{C}}\boldsymbol{V}\,\mathrm{d}\mathcal{S}. \tag{B22}$$

Variations result in

$$\begin{aligned} \omega_{AC}&=0, \quad \boldsymbol{\sigma}_{AC}=\alpha\left(1+\frac{\xi}{2}\beta\right)\boldsymbol{Id}_{\mathcal{S}}, & \boldsymbol{\eta}_{AC}&=\boldsymbol{0},\\ \boldsymbol{f}_{AC}&=\alpha\nabla\left(1+\frac{\xi}{2}\beta\right)=\frac{\alpha\xi}{2}\nabla\beta, & f^{\perp}_{AC}&=\alpha\left(1+\frac{\xi}{2}\beta\right)\mathcal{H}. \end{aligned} \tag{B23}$$

This means we only get an active pressure term, which has not any influence of the solution for an inextensible fluid and, thus, can be neglected. Although it is irrelevant for the present paper, it should be noted that $\boldsymbol{\sigma}_{AC}$ gives rise to geometric activity (Nitschke & Voigt 2025*a*) or active tension (Mietke *et al.* 2019; Wittwer & Aland 2023), respectively contributes to the membrane tension (Al-Izzi & Alexander 2023), depending on the scalar order in an extensible medium.

Appendix C. Energy rate

In this section we discuss the energy rate $(\mathrm{d}/\mathrm{d}t)\mathfrak{E}_{TOT}$ of the total energy

$$\mathfrak{E}_{TOT}:=\int_{\mathcal{S}}\frac{\rho}{2}\left\|\boldsymbol{V}\right\|^2_{T\mathbb{R}^3|_{\mathcal{S}}}\mathrm{d}\mathcal{S}+\mathfrak{U}_{LH}, \tag{C1}$$

consisting of the kinetic energy and the potential energy, the latter being given solely by the LH energy (4.25). Conceptually, one may either appeal to the intermediate result in Nitschke & Voigt (2025*b*) for the energy rate under the ansatz (4.1) or one may rederive it following the same procedure as in Nitschke & Voigt (2025*b*) within our framework. Either way, the Lagrange–d'Alembert principle yields the physical power balance

$$\frac{\mathrm{d}}{\mathrm{d}\mathfrak{E}}t_{TOT}=\mathfrak{P}_{TOT}=\mathfrak{P}_{NV}+\mathfrak{P}^{\Phi}_{IM}+\mathfrak{P}_{AC} \tag{C2}$$

for solutions of the governing equations (3.4), where the individual power inputs $\mathfrak{P}_\bullet$ due to anisotropic viscosity, immobility and activity fluxes are given by the product of generalised forces $(\boldsymbol{F}_\bullet,\boldsymbol{H}_\bullet)\in T\mathbb{R}^3|_{\mathcal{S}}\times\mathcal{Q}^2\mathbb{R}^3|_{\mathcal{S}}$, respectively $(\boldsymbol{f}_\bullet,f^{\perp}_\bullet,\omega_\bullet)\in T\mathcal{S}\times T^0\mathcal{S}\times T^0\mathcal{S}$,

https://doi.org/10.1017/jfm.2026.11474 Published online by Cambridge University Press

and generalised velocities $(\boldsymbol{V}, \mathrm{D}_t^{\mathfrak{m}}\, \boldsymbol{Q}) \in T\mathbb{R}^3|_{\mathcal{S}} \times \mathcal{Q}^2\mathbb{R}^3|_{\mathcal{S}}$, respectively $(\boldsymbol{v}, v_\perp, \dot\beta) \in T\mathcal{S} \times T^0\mathcal{S} \times T^0\mathcal{S}$, i.e.

$$\begin{aligned}\mathfrak{P}_\bullet &= \langle \boldsymbol{F}_\bullet, \boldsymbol{V}\rangle_{\mathrm{L}^2(T\mathbb{R}|_{\mathcal{S}})} + \big\langle \boldsymbol{H}_\bullet, \mathrm{D}_t^{\mathfrak{m}}\, \boldsymbol{Q}\big\rangle_{\mathrm{L}^2(\mathcal{Q}^2\mathbb{R}^3|_{\mathcal{S}})} = \big\langle \boldsymbol{f}_\bullet, \boldsymbol{v}\big\rangle_{\mathrm{L}^2(T\mathcal{S})} + \big\langle f_\bullet^\perp, v_\perp\big\rangle_{\mathrm{L}^2(T^0\mathcal{S})} \\ &\quad + \frac{3}{2}\big\langle \omega_\bullet, \dot\beta\big\rangle_{\mathrm{L}^2(T^0\mathcal{S})} \\ &= -\left(\langle \boldsymbol{\sigma}_\bullet, \nabla \boldsymbol{v} - v_\perp \boldsymbol{II}\rangle_{\mathrm{L}^2(T^2\mathcal{S})} + \big\langle \boldsymbol{\eta}_\bullet, \nabla v_\perp + \boldsymbol{II}\, \boldsymbol{v}\big\rangle_{\mathrm{L}^2(T\mathcal{S})} - \frac{3}{2}\big\langle \omega_\bullet, \dot\beta\big\rangle_{\mathrm{L}^2(T^0\mathcal{S})}\right) \end{aligned} \tag{C3}$$

with fluid stress fields $(\boldsymbol{\sigma}_\bullet, \boldsymbol{\eta}_\bullet) \in T^2\mathcal{S} \times T\mathcal{S}$ (B2). Inextensibility (3.4*c*) and stress/force (B15) result in $\mathfrak{P}_{NV} = -2\mathfrak{R}_{NV}$ (B14); stress/force (B20) yields $\mathfrak{P}_{IM}^\Phi = -2\mathfrak{R}_{IM}^\Phi$ (B19) for $\Phi \in \{\mathfrak{m}, \mathcal{J}\}$; the activity power/flux potential $\mathfrak{P}_{AC} = \mathfrak{R}_{AC} = 0$ vanishes as expected by (B23). Eventually, we summarise that

$$\begin{aligned}\frac{\mathrm{d}}{\mathrm{d}t}\mathfrak{E}_{TOT} &= -\frac{1}{4}\left(2\upsilon \left\| \left(1 + \frac{\xi}{2}\beta\right) \boldsymbol{Id}_{\mathcal{S}} \left(\nabla_{\mathsf{C}} \boldsymbol{V} + \nabla_{\mathsf{C}}^T \boldsymbol{V}\right) \boldsymbol{Id}_{\mathcal{S}} \right\|^2_{\mathrm{L}^2(T^2\mathcal{S})} \right. \\ &\qquad \left. + 3\left(2M + \upsilon\xi^2\right) \left\|\dot\beta\right\|^2_{\mathrm{L}^2(T^0\mathcal{S})} + 18M\delta_{\mathfrak{m}}^\phi \left\|\beta\nu\nabla_{\mathsf{C}}\boldsymbol{V}\right\|^2_{\mathrm{L}^2(T\mathcal{S})}\right) \\ &= -2\left(\mathfrak{R}_{NV} + \mathfrak{R}_{IM}^\Phi\right) \le 0 \end{aligned} \tag{C4}$$

for solutions of the LH model (3.4). Consequently, the evolution of both the surface $\mathcal{S}$ and the scalar order parameter β is of a purely dissipative nature. This dissipation is irreversible and, hence, directly proportional to the entropy production.

Appendix D. Surface-conforming Beris–Edwards model

In the following we merely recall the surface-conforming active Beris–Edwards model from Nitschke & Voigt (2025*a*). The full derivation and all mathematical background that is not reiterated here are provided in Nitschke & Voigt (2025*a*,*b*).

Find the tangential and normal material velocity fields $\boldsymbol{v} \in T\mathcal{S}$ and $v_\perp \in T^0\mathcal{S}$, tangential Q-tensor field $\boldsymbol{q} \in \mathcal{Q}^2\mathcal{S}$, normal eigenvalue field $\beta \in T^0\mathcal{S}$, pressure field $p \in T^0\mathcal{S}$ and Lagrange parameter fields $\boldsymbol{\lambda}_\gamma \in \mathcal{V}_\gamma \le T^n\mathbb{R}^3|_{\mathcal{S}}$ for all $\gamma \in \mathcal{C}_{SC}$ such that

$$\begin{aligned}\rho \boldsymbol{a} &= \nabla \tilde p + \operatorname{div}\left(\boldsymbol{\sigma}_{EL} + \boldsymbol{\sigma}_{IM}^\Phi + \boldsymbol{\sigma}_{NV}^0 + \xi\boldsymbol{\sigma}_{NV}^1 + \xi^2\boldsymbol{\sigma}_{NV}^2 + \boldsymbol{\sigma}_{NA}\right) \\ &\quad + (2\boldsymbol{II}\,\boldsymbol{q} - 3\beta\boldsymbol{II})\left(\boldsymbol{\zeta}_{EL} + \boldsymbol{\zeta}_{IM}^\Phi\right) + \sum_{\gamma\in\mathcal{C}_{SC}} \boldsymbol{f}_\gamma, \end{aligned} \tag{D1a}$$

$$\begin{aligned}\rho a_\perp &= \tilde p\mathcal{H} + f_{BE}^\perp + \boldsymbol{II} : \left(\boldsymbol{\sigma}_{EL} + \boldsymbol{\sigma}_{IM}^\Phi + \boldsymbol{\sigma}_{NV}^0 + \xi\boldsymbol{\sigma}_{NV}^1 + \xi^2\boldsymbol{\sigma}_{NV}^2 + \boldsymbol{\sigma}_{NA}\right) \\ &\quad - \operatorname{div}\left((2\boldsymbol{q} - 3\beta\boldsymbol{Id}_{\mathcal{S}})\left(\boldsymbol{\zeta}_{EL} + \boldsymbol{\zeta}_{IM}^\Phi\right)\right) + \sum_{\gamma\in\mathcal{C}_{SC}} f_\gamma^\perp, \end{aligned} \tag{D1b}$$

$$\left(M + \frac{\upsilon\xi^2}{2}\right) \mathrm{d}_t^\Phi\, \boldsymbol{q} = \boldsymbol{h}_{EL} + \boldsymbol{h}_{TH} + \xi\boldsymbol{h}_{NV}^1 + \xi^2\widetilde{\boldsymbol{h}}_{NV}^{2,\Phi} + \sum_{\gamma\in\mathcal{C}_{SC}} \boldsymbol{h}_\gamma, \tag{D1c}$$

$$\left(M + \frac{\upsilon\xi^2}{2}\right) \dot\beta = \omega_{\mathrm{EL}} + \omega_{\mathrm{TH}} + \xi^2\widetilde{\omega}_{NV}^2 + \sum_{\gamma\in\mathcal{C}_{SC}} \omega_\gamma, \tag{D1d}$$

$$\operatorname{div}\boldsymbol{v} = v_\perp\mathcal{H}, \tag{D1e}$$

$$\forall \gamma \in \mathcal{C}_{SC}: \quad \boldsymbol{0} = \boldsymbol{C}_\gamma \tag{D1f}$$

https://doi.org/10.1017/jfm.2026.11474 Published online by Cambridge University Press

holds for $\dot{\rho} = 0$ and given initial conditions for $\boldsymbol{v}$, $v_\perp$, $\boldsymbol{q}$, β and mass density $\rho \in T^0\mathcal{S}$.

Quantities are unpacked in table 5. The choice of Φ for $\boldsymbol{\sigma}^1_{NV}$ and $\boldsymbol{\sigma}^2_{NV}$ is optional. Both given representations state equal tensor fields. Here $\mathcal{C}_{SC}$ is a set of constraints suitable for surface-conforming Q-tensor fields, which might yield additional constraint forces. In this paper we only consider the 'no flat degeneracy' (ND) constraint, i.e. $\mathcal{C}_{SC} = \{\mathrm{ND}\}$ holds and $\boldsymbol{f}_{ND}$, $f^\perp_{ND}$, $\boldsymbol{h}_{ND}$, ω_{ND}, $\boldsymbol{C}_{ND}$ are the associated generalised constraint forces derived in Appendix E. Since this is an inextensible model, we summarise obvious pressure terms into the generalised pressure $\tilde{p} \in T^0\mathcal{S}$ for simplicity.

Appendix E. No flat degeneracy constraint

The 'no flat degeneracy' constraint may be given by

$$\mathbf{0} = \boldsymbol{q} = (\Pi_{\mathcal{Q}^2\mathcal{S}} \circ \Pi_{T^2\mathcal{S}})\,\boldsymbol{Q} = \boldsymbol{Id}_{\mathcal{S}}\,\boldsymbol{Q}\,\boldsymbol{Id}_{\mathcal{S}} - \frac{\boldsymbol{Q} : \boldsymbol{Id}_{\mathcal{S}}}{2}\boldsymbol{Id}_{\mathcal{S}} = \boldsymbol{C}_{ND}, \tag{E1}$$

where $\Pi_{T^2\mathcal{S}} : T^2\mathbb{R}^3|_{\mathcal{S}} \to T^2\mathcal{S}$ is the orthogonal tangential projection on two-tensor fields with $\Pi_{T^2\mathcal{S}}\boldsymbol{R} = \boldsymbol{Id}_{\mathcal{S}}\boldsymbol{R}\boldsymbol{Id}_{\mathcal{S}}$ for all $\boldsymbol{R} \in T^2\mathbb{R}^3|_{\mathcal{S}}$, and $\Pi_{\mathcal{Q}^2\mathcal{S}} : T^2\mathcal{S} \to \mathcal{Q}^2\mathcal{S}$ is the orthogonal flat-degenerated Q-tensor projection on tangential two-tensor fields with $\Pi_{\mathcal{Q}^2\mathcal{S}}\boldsymbol{r} = (1/2)(\boldsymbol{r} + \boldsymbol{r}^T - (\mathrm{Tr}\boldsymbol{r})\boldsymbol{Id}_{\mathcal{S}})$. To implement this into the surface-conforming model (D1), we introduce the Lagrange functional

$$\mathfrak{U}_{ND} := -\left\langle \boldsymbol{\lambda}_{ND},\, (\Pi_{\mathcal{Q}^2\mathcal{S}} \circ \Pi_{T^2\mathcal{S}})\,\boldsymbol{Q}\right\rangle_{\mathrm{L}^2(\mathcal{Q}^2\mathcal{S})} = -\left\langle \boldsymbol{\lambda}_{ND},\, \boldsymbol{Q}\right\rangle_{\mathrm{L}^2(\mathcal{Q}^2\mathbb{R}^3|_{\mathcal{S}})} \tag{E2}$$

as a potential energy, with Lagrange parameter $\boldsymbol{\lambda}_{ND} \in \mathcal{Q}^2\mathcal{S}$ yielding an additional degree of freedom. The variation

$$\langle \boldsymbol{C}_{ND}, \boldsymbol{\theta}\rangle_{\mathrm{L}^2(\mathcal{Q}^2\mathcal{S})} := -\left\langle \frac{\delta\mathfrak{U}_{ND}}{\delta\boldsymbol{\lambda}_{ND}}, \boldsymbol{\theta}\right\rangle_{\mathrm{L}^2(\mathcal{Q}^2\mathcal{S})} = 0 \tag{E3}$$

for all virtual displacements $\boldsymbol{\theta} \in \mathcal{Q}^2\mathcal{S}$ results in the constraint equation (E1). The molecular constraint force $\boldsymbol{H}_{ND} \in \mathcal{Q}^2\mathbb{R}^3|_{\mathcal{S}}$ is given by the variation

$$\langle \boldsymbol{H}_{ND}, \boldsymbol{\Psi}\rangle_{\mathrm{L}^2(\mathcal{Q}^2\mathbb{R}^3|_{\mathcal{S}})} := -\left\langle \frac{\delta\mathfrak{U}_{ND}}{\delta\boldsymbol{Q}}, \boldsymbol{\Psi}\right\rangle_{\mathrm{L}^2(\mathcal{Q}^2\mathbb{R}^3|_{\mathcal{S}})} = \langle \boldsymbol{\lambda}_{ND}, \boldsymbol{\Psi}\rangle_{\mathrm{L}^2(\mathcal{Q}^2\mathbb{R}^3|_{\mathcal{S}})} \tag{E4}$$

for all virtual displacements $\boldsymbol{\Psi} \in \mathcal{Q}^2\mathbb{R}^3|_{\mathcal{S}}$. Therefore, the constraint force is flat degenerated and we have to add

$$\boldsymbol{h}_{ND} := (\Pi_{\mathcal{Q}^2\mathcal{S}} \circ \Pi_{T^2\mathcal{S}})\,\boldsymbol{H}_{ND} = \boldsymbol{H}_{ND} = \boldsymbol{\lambda}_{ND} \in \mathcal{Q}^2\mathcal{S} \tag{E5}$$

to the right-hand side of the flat-degenerated molecular equation (D1c). Since $\boldsymbol{\lambda}_{ND}$ is fully determined by that equation, we can, in principle, omit it. However, as is the case with the surface-conforming constraint in Nitschke & Voigt (2025*b*), an additional constraint force $\boldsymbol{F}_{ND} = \boldsymbol{f}_{ND} + f^\perp_{ND}\boldsymbol{\nu}$ may need to be accounted for in the fluid equations (D1*a*) and (D1*b*). Spatial state variation yields

$$\begin{aligned}
&\langle \boldsymbol{F}_{ND}, \boldsymbol{W}\rangle_{\mathrm{L}^2(T\mathbb{R}^3|_{\mathcal{S}})} := -\left\langle \frac{\delta\mathfrak{U}_{ND}}{\delta\boldsymbol{X}}, \boldsymbol{W}\right\rangle_{\mathrm{L}^2(T\mathbb{R}^3|_{\mathcal{S}})} \\
&= \int_{\mathcal{S}} \eth_{\boldsymbol{W}}\,\langle \boldsymbol{\lambda}_{ND}, \boldsymbol{q}\rangle_{\mathcal{Q}^2\mathcal{S}} + \langle \boldsymbol{\lambda}_{ND}, \boldsymbol{q}\rangle_{\mathcal{Q}^2\mathcal{S}}\,(\mathrm{Div}_{\mathsf{C}}\boldsymbol{W})\mathrm{d}\mathcal{S} \\
&= \langle \eth_{\boldsymbol{W}}\boldsymbol{\lambda}_{ND} + (\mathrm{Div}_{\mathsf{C}}\boldsymbol{W})\boldsymbol{\lambda}_{ND}, \boldsymbol{q}\rangle_{\mathrm{L}^2(\mathcal{Q}^2\mathbb{R}^3|_{\mathcal{S}})} + \left\langle \boldsymbol{\lambda}_{ND}, (\eth_{\boldsymbol{W}} \circ \Pi_{\mathcal{Q}^2\mathcal{S}} \circ \Pi_{T^2\mathcal{S}})\,\boldsymbol{Q}\right\rangle_{\mathrm{L}^2(\mathcal{Q}^2\mathbb{R}^3|_{\mathcal{S}})}
\end{aligned} \tag{E6}$$

https://doi.org/10.1017/jfm.2026.11474 Published online by Cambridge University Press

for all virtual displacements $\boldsymbol{W} \in T\mathbb{R}^3|_{\mathcal{S}}$ and $\boldsymbol{q} = (\Pi_{\mathcal{Q}^2\mathcal{S}} \circ \Pi_{T^2\mathcal{S}})\, \boldsymbol{Q}$. The first summand vanishes due to constraint (E1). For the second summand, we use the identity (Nitschke *et al.* 2023)

$$\eth_{\boldsymbol{W}} \boldsymbol{Id}_{\mathcal{S}} = \eth_{\boldsymbol{W}} (\boldsymbol{Id} - \boldsymbol{\nu} \otimes \boldsymbol{\nu}) = -\eth_{\boldsymbol{W}} \boldsymbol{\nu} \otimes \boldsymbol{\nu} - \boldsymbol{\nu} \otimes \eth_{\boldsymbol{W}} \boldsymbol{\nu} = \boldsymbol{\nu}(\nabla_{\mathsf{C}} \boldsymbol{W}) \otimes \boldsymbol{\nu} + \boldsymbol{\nu} \otimes \boldsymbol{\nu} \nabla_{\mathsf{C}} \boldsymbol{W}, \tag{E7}$$

and obtain, by means of (E1), that

$$\begin{aligned}
&\left(\Pi_{\mathcal{Q}^2\mathcal{S}} \circ \Pi_{T^2\mathcal{S}} \circ \eth_{\boldsymbol{W}} \circ \Pi_{\mathcal{Q}^2\mathcal{S}} \circ \Pi_{T^2\mathcal{S}}\right) \boldsymbol{Q} \\
&\quad = \left(\Pi_{\mathcal{Q}^2\mathcal{S}} \circ \Pi_{T^2\mathcal{S}}\right) \Big(\boldsymbol{Id}_{\mathcal{S}} \eth_{\boldsymbol{W}} \boldsymbol{Q} \boldsymbol{Id}_{\mathcal{S}} + \eth_{\boldsymbol{W}} \boldsymbol{Id}_{\mathcal{S}} \boldsymbol{Q} \boldsymbol{Id}_{\mathcal{S}} + \boldsymbol{Id}_{\mathcal{S}} \boldsymbol{Q} \eth_{\boldsymbol{W}} \boldsymbol{Id}_{\mathcal{S}} \\
&\qquad - \frac{\eth_{\boldsymbol{W}} \boldsymbol{Q} : \boldsymbol{Id}_{\mathcal{S}} + \boldsymbol{Q} : \eth_{\boldsymbol{W}} \boldsymbol{Id}_{\mathcal{S}}}{2} \boldsymbol{Id}_{\mathcal{S}} - \frac{\boldsymbol{Q} : \boldsymbol{Id}_{\mathcal{S}}}{2} \eth_{\boldsymbol{W}} \boldsymbol{Id}_{\mathcal{S}} \Big) \\
&\quad = \left(\Pi_{\mathcal{Q}^2\mathcal{S}} \circ \Pi_{T^2\mathcal{S}}\right) \Big(\boldsymbol{Id}_{\mathcal{S}} \eth_{\boldsymbol{W}} \boldsymbol{Q} \boldsymbol{Id}_{\mathcal{S}} + \boldsymbol{\nu} \otimes \boldsymbol{\nu}(\nabla_{\mathsf{C}} \boldsymbol{W})\, \boldsymbol{Q} \boldsymbol{Id}_{\mathcal{S}} + \boldsymbol{Id}_{\mathcal{S}} \boldsymbol{Q} (\boldsymbol{\nu}(\nabla_{\mathsf{C}} \boldsymbol{W})) \otimes \boldsymbol{\nu} \\
&\qquad - \frac{\eth_{\boldsymbol{W}} \boldsymbol{Q} : \boldsymbol{Id}_{\mathcal{S}}}{2} \boldsymbol{Id}_{\mathcal{S}} - \frac{\boldsymbol{Q} : \boldsymbol{Id}_{\mathcal{S}}}{2} \left(\boldsymbol{\nu}(\nabla_{\mathsf{C}} \boldsymbol{W}) \otimes \boldsymbol{\nu} + \boldsymbol{\nu} \otimes \boldsymbol{\nu} \nabla_{\mathsf{C}} \boldsymbol{W}\right) \Big) \\
&\quad = \left(\Pi_{\mathcal{Q}^2\mathcal{S}} \circ \Pi_{T^2\mathcal{S}}\right) \Big(\boldsymbol{Id}_{\mathcal{S}} \eth_{\boldsymbol{W}} \boldsymbol{Q} \boldsymbol{Id}_{\mathcal{S}} - \frac{\eth_{\boldsymbol{W}} \boldsymbol{Q} : \boldsymbol{Id}_{\mathcal{S}}}{2} \boldsymbol{Id}_{\mathcal{S}} \Big) = \left(\Pi_{\mathcal{Q}^2\mathcal{S}} \circ \Pi_{T^2\mathcal{S}}\right) \eth_{\boldsymbol{W}} \boldsymbol{Q}
\end{aligned} \tag{E8}$$

holds, since, *a priori*, $\boldsymbol{Q}$ is surface conforming and, thus, cannot have tangential-normal, respectively normal-tangential, components. Eventually, the spatial state variation results in

$$\langle \boldsymbol{F}_{ND}, \boldsymbol{W} \rangle_{\mathrm{L}^2(T\mathbb{R}^3|_{\mathcal{S}})} = \langle \boldsymbol{\lambda}_{ND}, \eth_{\boldsymbol{W}} \boldsymbol{Q} \rangle_{\mathrm{L}^2(\mathcal{Q}^2\mathbb{R}^3|_{\mathcal{S}})} = \langle \boldsymbol{H}_{ND}, \eth_{\boldsymbol{W}} \boldsymbol{Q} \rangle_{\mathrm{L}^2(\mathcal{Q}^2\mathbb{R}^3|_{\mathcal{S}})}\,. \tag{E9}$$

This gives a pure 'gauge of surface independence' force with respect to $\boldsymbol{Q}$; cf. Nitschke *et al.* (2023). Such gauge forces can be ignored, since the net gauge force is balanced within the fluid equation, independently of the choice of $\eth_{\boldsymbol{W}} \boldsymbol{Q}$; see Nitschke & Voigt (2025*b*). Therefore, we choose $\eth_{\boldsymbol{W}} \boldsymbol{Q} = \boldsymbol{0}$ without loss of generality, and obtain $\boldsymbol{F}_{ND} = \boldsymbol{0}$, i.e. no additional constraint forces have to be considered in (D1*a*) and (D1*b*). To summarise the implications: in order to apply the 'no flat degeneracy' constraint (E1) to the surface-conforming model (D1) without using the Lagrange multiplier $\boldsymbol{\lambda}_{ND}$, it suffices to omit the flat-degenerated molecular equation (D1*c*) and substitute $\boldsymbol{q} = \boldsymbol{0}$ throughout the remaining model.

Appendix F. Numerical realisation

The numerical approach to solve the surface Beris–Edwards model for symmetric bilayers (3.1) and the hydrodynamic surface LH model for asymmetric bilayers (3.4) extends the approach used in Krause & Voigt (2023) for (3.8) and Bachini *et al.* (2023*a*), Sischka & Voigt (2025) for surface two-phase systems. We consider a surface finite element method (Dziuk & Elliott 2013; Nestler *et al.* 2019) within an Arbitrary Lagrangian–Eulerian approach (Krause & Voigt 2023; Sauer 2025). This includes a mesh redistribution approach (Barrett, Garcke & Nurnberg 2008) for which the systems are extended by equations for the surface parametrisation

$$\partial_t \boldsymbol{X} \cdot \boldsymbol{\nu} = \boldsymbol{V} \cdot \boldsymbol{\nu}, \tag{F1}$$

$$\mathcal{H} \boldsymbol{\nu} = \Delta_C \boldsymbol{X}, \tag{F2}$$

which generate a tangential mesh movement to maintain shape regularity and additionally provide an implicit representation of the mean curvature $\mathcal{H}$.

https://doi.org/10.1017/jfm.2026.11474 Published online by Cambridge University Press

The implementation is done in DUNE/AMDiS (Vey & Voigt 2007; Witkowski *et al.* 2015; Blatt *et al.* 2025) using the DUNECurvedGrid library (Praetorius & Stenger 2022). We consider a discrete kth order approximation $\mathcal{S}_h^k$ of $\mathcal{S}$, with h the size of the mesh elements, i.e. the longest edge of the mesh, and consider each geometrical quantity like the normal vector $\boldsymbol{\nu}_h$, the identity $\boldsymbol{Id}_{\mathcal{S},h}$, the shape operator $\boldsymbol{II}_h$ and the Gaussian curvature $\mathcal{K}_h$ with respect to $\mathcal{S}_h^k$. We define the discrete function spaces for scalar functions by $W_k\mathcal{S}_h^k) = \{\psi \in C^0(\mathcal{S}_h^k) | \psi|_T \in \mathcal{P}_k(T)\}$ and for vector fields by $\boldsymbol{W}_k(\mathcal{S}_h^k) = [W_k(\mathcal{S}_h^k)]^3$. Within these definitions T is the mesh element and $\mathcal{P}_k$ are the polynomials of order k. We consider $\boldsymbol{V}_h, \boldsymbol{X} \in \boldsymbol{W}_2(\mathcal{S}_h^k)$, $\mathcal{H}_h, \beta_h \in W_1(\mathcal{S}_h^k)$ and $p_h \in W_1(\mathcal{S}_h^k)$, which leads to an isogeometric setting and a $\mathcal{P}_2 - \mathcal{P}_1$ Taylor–Hood element for the surface Navier–Stokes-like equations. We discretise in time using semi-implicit time stepping with constant step size τ. We use an operator splitting approach. In each time step we first solve the equation for the orientation field and then solve the surface Navier–Stokes-like equations and the mesh redistribution together. Then, we update the surface, lifting the solutions $\boldsymbol{V}_h^n$, $\tilde{p}_h^n$, $\mathcal{H}_h^n$ and β_h^n to the new surface and computing the remaining geometric quantities $\boldsymbol{\nu}_h^n$, $\boldsymbol{Id}_{\mathcal{S},h}$ $\boldsymbol{II}_h^n$ and $\mathcal{K}_h^n$ for the new surface. To resolve the nonlinear terms in the dynamic of the orientation field, we consider all surface quantities from the previous time step and consider a one-step Picard iteration for the terms nonlinear in β. For the surface dynamic, we consider $\boldsymbol{\nu}_h$, $\boldsymbol{Id}_{\mathcal{S},h}$, $\boldsymbol{II}_h$ and $\mathcal{K}_h$ explicitly and resolve the nonlinearity in the material acceleration $(\boldsymbol{\nabla}_{\mathsf{C}}\boldsymbol{V}_h)\boldsymbol{V}_h$ by considering $\boldsymbol{\nabla}_{\mathsf{C}}\boldsymbol{V}_h$ implicitly and $\boldsymbol{V}_h$ explicitly. For convergence studies of the surface Navier–Stokes equations with this approach, we refer to Krause & Voigt (2023), for such studies with similar coupling terms with surface scalar quantities, we refer to Bachini *et al.* (2023*a*) and for corresponding treatments of Gaussian curvature terms, see Sischka & Voigt (2025) and Sischka *et al.* (2025).

In order to explore the differences between the surface Beris–Edwards model and the hydrodynamic surface LH model with the corresponding surface Navier–Stokes–Helfrich models, we consider an initial surface $\mathcal{S}_0$ as a perturbed unit sphere, i.e.

$$\mathcal{S}_0 = \left\{1 + r_0 Y_l^m(\phi, \vartheta) : \phi \in [0, \pi], \vartheta \in [-\pi, \pi]\right\}, \quad r_0 > 0, \tag{F3}$$

$$Y_l^m(\phi, \vartheta) = \sqrt{\frac{2l+1(l-m)!}{4\pi(l+m)!}} P_l^m(\cos\vartheta) \mathrm{e}^{im\phi}, \tag{F4}$$

with spherical harmonics Y_l^m and Legendre polynomials P_l^m and the case $l = 5$, $m = 3$ and $r_0 = 0.5$. The velocity field is initialised with $\boldsymbol{V}_0 = 0$, the scalar order field with $\beta_0 = (2/3)$. The initial surface has a non-zero mean and Gaussian curvature and is out of equilibrium.

As physical parameters, we choose $\xi = 0$, $\upsilon = M = \rho = 1$ and $L = 0.1$. In the case of the surface Beris–Edwards model (3.1) we further consider $a = 0$, $b = -27$ and $c = (27/2)$, in the case of the hydrodynamic surface LH model (3.4), we choose $\hat{a} = 0$, $\varpi = 1$ and $\kappa = \bar{\kappa} = 0.2$ leading to comparable conditions (c.f. (3.5)). In the hydrodynamic surface LH model, we further choose $\mathcal{H}_0 = -1.77$, which corresponds to the mean curvature of the expected equilibrium shape of $\mathcal{S}$ for both systems, a sphere with radius $r = 1.129$. We further consider $\hat{\mathcal{H}}_0 = 0$. Numerical parameters, such as mesh size h and time step τ are chosen to resolve the highest curvature values and to meet stability constraints, following Krause & Voigt (2023), Bachini *et al.* (2023*a*), Sischka & Voigt (2025). To study the influence of the orientation field β on the system, we also solve the surface Navier–Stokes–Helfrich model (3.8) with either $H_0 = 0$ for the symmetric case or $H_0 = -1.77$ for the asymmetric case and all other parameters chosen as stated above.

https://doi.org/10.1017/jfm.2026.11474 Published online by Cambridge University Press

References

Al-Izzi, S.C. & Alexander, G.P. 2023 Chiral active membranes: odd mechanics, spontaneous flows, and shape instabilities. *Phys. Rev. Res.* **5** (4), 043227.

Alexe-Ionescu, A.L. 1993 Flexoelectric polarization and second order elasticity for nematic liquid crystals. *Phys. Lett. A* **180** (6), 456–460.

Arroyo, M. & DeSimone, A. 2009 Relaxation dynamics of fluid membranes. *Phys. Rev. E* **79** (3), 031915.

Bachini, E., Krause, V., Nitschke, I. & Voigt, A. 2023*a* Derivation and simulation of a two-phase fluid deformable surface model. *J. Fluid Mech.* **977**, 031915.

Bachini, E., Krause, V. & Voigt, A. 2023*b* The interplay of geometry and coarsening in multicomponent lipid vesicles under the influence of hydrodynamics. *Phys. Fluids* **35** (4), 042102.

Barbero, G., Dozov, I., Palierne, J.F. & Durand, G. 1986 Order electricity and surface orientation in nematic liquid crystals. *Phys. Rev. Lett.* **56** (19), 2056–2059.

Barrett, J.W., Garcke, H. & Nurnberg, R. 2008 Parametric approximation of Willmore flow and related geometric evolution equations. *SIAM J. Sci. Comput.* **31** (1), 225–253.

Barrett, J.W., Garcke, H. & Nürnberg, R. 2017 Finite element approximation for the dynamics of fluidic two-phase biomembranes. *ESAIM: Math. Modell. Numer. Anal.* **51** (6), 2319–2366.

Bartels, S., Dolzmann, G., Nochetto, R.H. & Raisch, A. 2012 Finite element methods for director fields on flexible surfaces. *Interfaces Free Bound.* **14** (2), 231–272.

Baumgart, T., Hess, S.T. & Webb, W.W. 2003 Imaging coexisting fluid domains in biomembrane models coupling curvature and line tension. *Nature* **425** (6960), 821–824.

Beris, A.N. & Edwards, B.J. 1994 *Thermodynamics of Flowing Systems: with Internal Microstructure*. Oxford University Press.

Blatt, M., *et al.* 2025 The Distributed and Unified Numerics Environment (DUNE), Version 2.10. arXiv:2506.23558

Bogdanov, M., Pyrshev, K., Yesylevskyy, S., Ryabichko, S., Boiko, V., Ivanchenko, P., Kiyamova, R., Guan, Z., Ramseyer, C. & Dowhan, W. 2020 Phospholipid distribution in the cytoplasmic membrane of Gram-negative bacteria is highly asymmetric, dynamic, and cell shape-dependent. *Sci. Adv.* **6** (23), eaaz6333.

Brandner, P., Reusken, A. & Schwering, P. 2022 On derivations of evolving surface Navier–Stokes equations. *Interfaces Free Bound.* **24** (4), 533–563.

Dimova, R., Aranda, S., Bezlyepkina, N., Nikolov, V., Riske, K.A. & Lipowsky, R. 2006 A practical guide to giant vesicles. Probing the membrane nanoregime via optical microscopy. *J. Phys.: Condens. Matter* **18** (28), S1151–S1176.

Dziuk, G. & Elliott, C.M. 2013 Finite element methods for surfaces PDEs. *Acta Numer.* **22**, 289–396.

Elliott, C.M. & Stinner, B.örn 2010 A surface phase field model for two-phase biological membranes. *SIAM J. Appl. Math.* **70** (8), 2904–2928.

Enoki, T.A. & Heberle, F.A. 2023 Experimentally determined leaflet–leaflet phase diagram of an asymmetric lipid bilayer. *Proc. Acad. Nat. Sci.* **120** (46), e2308723120.

Faizi, H.A., Dimova, R. & Vlahovska, P. 2021 A vesicle microrheometer for high-throughput viscosity measurements of lipid and polymer membranes. *Biophys. J.* **121** (6), 910–918.

Ghosh, R., Satarifard, V., Grafmüller, A. & Lipowsky, R. 2019 Spherical nanovesicles transform into a multitude of nonspherical shapes. *Nano Lett.* **19** (11), 7703–7711.

Govers, E. & Vertogen, G. 1984 Elastic continuum theory of biaxial nematics. *Phys. Rev. A* **30** (4), 1998–2000.

Helfrich, W. 1971 The strength of piezoelectricity in liquid crystals. *Z. Naturforsch. A* **26** (5), 833–835.

Helfrich, W. 1973 Elastic properties of lipid bilayers: theory and possible experiments. *Z. Naturforsch. C* **28** (11–12), 693–703.

Hu, D., Zhang, P. & Weinan, E. 2007 Continuum theory of a moving membrane. *Phys. Rev. E* **75** (4), 041605.

Jülicher, F. & Lipowsky, R. 1996 Shape transformations of vesicles with intramembrane domains. *Phys. Rev. E* **53** (3), 2670.

Kahraman, O., Langen, R. & Haselwandter, C.A. 2018 Directed supramolecular organization of N-BAR proteins through regulation of H0 membrane immersion depth. *Sci. Rep-UK* **8** (1), 16383.

Kirchhausen, T. 2012 Bending membranes. *Nat. Cell Biol.* **14** (9), 906–908.

Krause, V. & Voigt, A. 2023 A numerical approach for fluid deformable surfaces with conserved enclosed volume. *J. Comput. Phys.* **486**, 112097.

https://doi.org/10.1017/jfm.2026.11474 Published online by Cambridge University Press

LIPOWSKY, R., GHOSH, R., SATARIFARD, V., SREEKUMARI, A., ZAMALETDINOV, M., RÓŻYCKI, B., MIETTINEN, M. & GRAFMÜLLER, A. 2023 Leaflet tensions control the spatio-temporal remodeling of lipid bilayers and nanovesicles. *Biomolecules* **13** (6), 926.

LONDON, E. 2019 Membrane structure–function insights from asymmetric lipid vesicles. *Accounts Chem. Res.* **52** (8), 2382–2391.

LORENT, J.H., LEVENTAL, K.R., GANESAN, L., RIVERA-LONGSWORTH, G., SEZGIN, E., DOKTOROVA, M., LYMAN, E. & LEVENTAL, I. 2020 Plasma membranes are asymmetric in lipid unsaturation, packing and protein shape. *Nat. Chem. Biol.* **16** (6), 644–652.

LOWENGRUB, J.S., RÄTZ, A. & VOIGT, A. 2009 Phase-field modeling of the dynamics of multicomponent vesicles: spinodal decomposition, coarsening, budding, and fission. *Phys. Rev. E* **79**, 031926.

MARSH, D. 2013 *Handbook of Lipid Bilayers*. CRC Press.

MCMAHON, H.T. & GALLOP, J.L. 2005 Membrane curvature and mechanisms of dynamic cell membrane remodelling. *Nature* **438** (7068), 590–596.

MEYER, R.B. 1969 Piezoelectric effects in liquid crystals. *Phys. Rev. Lett.* **22** (18), 918–921.

MIETKE, A., JEMSEENA, V., KUMAR, K.V., SBALZARINI, I.F. & JÜLICHER, F. 2019 Minimal model of cellular symmetry breaking. *Phys. Rev. Lett.* **123** (18), 188101.

MIRONOV, A.A., MIRONOV, A., DERGANC, J. & BEZNOUSSENKO, G.V. 2020 Membrane curvature, transmembrane area asymmetry, budding, fission and organelle geometry. *Intl J. Mol. Sci.* **21** (20), 7594.

MORI, H., Jr., GARTLAND, E.C., KELLY, J.R. & BOS, P.J. 1999 Multidimensional director modeling using the Q tensor representation in a liquid crystal cell and its application to the π cell with patterned electrodes. *Jpn. J. Appl. Phys.* **38** (1R), 135.

MOTTRAM, N.J. & NEWTON, C.J.P. 2014 Introduction to Q-tensor theory. arXiv:1409.3542.

NESTLER, M., NITSCHKE, I. & VOIGT, A. 2019 A finite element approach for vector-and tensor-valued surface PDEs. *J. Comput. Phys.* **389**, 48–61.

NITSCHKE, I. 2025 Moving surfaces: calculus of tensor fields, time derivatives and variations. Doctoral thesis, Technische Universität Dresden, urn: nbn: de: bsz: 14-qucosa2-950635.

NITSCHKE, I., NESTLER, M., PRAETORIUS, S., LÖWEN, H. & VOIGT, A. 2018 Nematic liquid crystals on curved surfaces: a thin film limit. *Proc. R. Soc. A* **474** (2214), 20170686.

NITSCHKE, I., REUTHER, S. & VOIGT, A. 2020 Liquid crystals on deformable surfaces. *Proc. R. Soc. A* **476** (2241), 20200313.

NITSCHKE, I., SADIK, S. & VOIGT, A. 2023 Tangential tensor fields on deformable surfaces — how to derive consistent L^2-gradient flows. *IMA J. Appl. Math.* **88** (6), 917–958.

NITSCHKE, I. & VOIGT, A. 2023 Tensorial time derivatives on moving surfaces: general concepts and a specific application for surface Landau–de Gennes models. *J. Geom. Phys.* **194**, 105002.

NITSCHKE, I. & VOIGT, A. 2025*a* Active nematodynamics on deformable surfaces. *Proc. R. Soc. A* **481** (2310), 20240380.

NITSCHKE, I. & VOIGT, A. 2025*b* Beris–Edwards models on evolving surfaces: a Lagrange-D'Alembert approach. *Adv. Differ. Equ.* **5** (6), 335–420.

OLSHANSKII, M.A. 2023 On equilibrium states of fluid membranes. *Phys. Fluids* **35** (6), 062111.

PRAETORIUS, S. & STENGER, F. 2022 Dune-CurvedGrid – A Dune module for surface parametrization. *Arch. Numer. Softw.* **6**, 1–27.

REUTHER, S., NITSCHKE, I. & VOIGT, A. 2020 A numerical approach for fluid deformable surfaces. *J. Fluid Mech.* **900**, R8.

RÓŻYCKI, B. & LIPOWSKY, R. 2015 Spontaneous curvature of bilayer membranes from molecular simulations: asymmetric lipid densities and asymmetric adsorption. *J. Chem. Phys.* **142** (5), 054101.

SALEEM, M., MORLOT, S., HOHENDAHL, A., MANZI, J., LENZ, M. & ROUX, A.ÉLIEN 2015 A balance between membrane elasticity and polymerization energy sets the shape of spherical clathrin coats. *Nat. Commun.* **6** (1), 6249.

SAUER, R.A. 2025 A curvilinear surface ALE formulation for self-evolving Navier–Stokes manifolds—general theory and analytical solutions. *J. Fluid Mech.* **1016**, A34.

SEIFERT, U. 1993 Curvature-induced lateral phase segregation in two-component vesicles. *Phys. Rev. Lett.* **70**, 1335–1338.

SEIFERT, U. 1997 Configurations of fluid membranes and vesicles. *Adv. Phys.* **46** (1), 13–137.

SISCHKA, J.M., NITSCHKE, I. & VOIGT, A. 2025 The influence of higher order geometric terms on the asymmetry and dynamics of membranes. *Faraday Discuss.* **259**, 454–474.

SISCHKA, J.M. & VOIGT, A. 2025 Two-phase fluid deformable surfaces with constant enclosed volume and phase-dependent bending and Gaussian rigidity. *Comput. Meth. Appl. Mech. Engng* **445**, 118166.

SREEKUMARI, A. & LIPOWSKY, R. 2018 Lipids with bulky head groups generate large membrane curvatures by small compositional asymmetries. *J. Chem. Phys.* **149** (8), 084901.

https://doi.org/10.1017/jfm.2026.11474 Published online by Cambridge University Press

SREEKUMARI, A. & LIPOWSKY, R. 2022 Large stress asymmetries of lipid bilayers and nanovesicles generate lipid flip-flops and bilayer instabilities. *Soft Matt.* **18** (32), 6066–6078.

TANIGUCHI, T. 1996 Shape deformation and phase separation dynamics of two-component vesicles. *Phys. Rev. Lett.* **76**, 4444–4447.

TORRES-SÁNCHEZ, A., MILLÁN, D. & ARROYO, M. 2019 Modelling fluid deformable surfaces with an emphasis on biological interfaces. *J. Fluid Mech.* **872**, 218–271.

VEY, S. & VOIGT, A. 2007 AMDiS: adaptive multidimensional simulations. *Comput. Vis. Sci.* **10**, 57–67.

WITKOWSKI, T., LING, S., PRAETORIUS, S. & VOIGT, A. 2015 Software concepts and numerical algorithms for a scalable adaptive parallel finite element method. *Adv. Comput. Math.* **41**, 1145–1177.

WITTWER, L.D. & ALAND, S. 2023 A computational model of self-organized shape dynamics of active surfaces in fluids. *J. Comput. Phys. X* **17**, 100126.

ZHU, C., SAINTILLAN, D. & CHERN, A. 2025 Stokes flow of an evolving fluid film with arbitrary shape and topology. *J. Fluid Mech.* **1003**, R1.

ZIMMERBERG, J. & KOZLOV, M.M. 2005 How proteins produce cellular membrane curvature. *Nat. Rev. Mol. Cell Bio.* **7** (1), 9–19.

https://doi.org/10.1017/jfm.2026.11474 Published online by Cambridge University Press